Title

MODERN METALLOGRAPHIC TECHNIQUES; LECTURES 4 AND 5: LECTURES FOR 2nd CONFERENCE ON MATERIALS SCIENCE, TRE-MEZZO, ITALY, SEPTEMBER 14-25, 1970

Author

Thomas, G.

Publication Date

1970-11-01

Lectures for 2nd Conference
on Materials Science, Tremezzo,
Italy, September 14-25, 1970

UCRL-19697
Preprint

LECTURES 4 AND 5: MODERN METALLOGRAPHIC TECHNIQUES

G. Thomas

November 1970

AEC Contract No. W-7405-eng-48

LAWRENCE RADIATION LABORATORY
UNIVERSITY of CALIFORNIA BERKELEY

UCRL-19697

DISCLAIMER

UCRL-19697

LECTURES 4 AND 5: MODERN METALLOGRAPHIC TECHNIQUES

G. Thomas

Inorganic Materials Research Division, Lawrence Radiation Laboratory
Department of Materials Science and Engineering, College of Engineering
University of California, Berkeley, California

1. Introduction

Metallography is the branch of metallurgy which is concerned with the study of structure and constitution of solid metals and alloys and its relation to the properties of these materials and also to their manufacture and treatment.

The structure of materials can be studied directly by various microscopical methods (fig. 1). The ability to resolve features of the structure depends on the specimen, the wavelength of the illumination used, and the efficiency of the optical system, i.e., the perfection of the lenses used in the microscope. The resolvable separation d of two objects is given by the well known optical relationship

$$d = \frac{0.61\ \lambda}{\mu \sin \alpha} = \frac{0.61\ \lambda}{N}$$

where λ = wavelength, μ = refractive index, and $\mu \sin \alpha = N$ is the numerical aperture of the lens. In order to improve resolution it is obvious that λ should be made as small as possible and N as large as possible. For light optics the following resolutions can be obtained:

white light, $\lambda = 4200\text{Å}$ $\quad N = 1.4$ (oil immersion) $\quad d = 1800\text{Å}$

ultraviolet light, $\lambda = 2537\text{Å}$ $\quad N = 1.4$ $\quad d = 1100\text{Å}$

The optimum resolution in light optics is thus ~ 1000Å. Smaller wavelengths are possible by using x-rays and electrons. In the former case lenses for refracting x-rays are impractical but in the latter case electromagnetic or electrostatic lenses can be used to focus electron beams. Unfortunately electron lenses cannot be made with large aperture

TABLE 1

Technique and Specimen needed	Resolution	Useful Range of Detectable Density of Lattice Defects*		
		Point	Line	Surface
Field Ion: wire: tip radius 300 atoms	2-3Å	Individual point defects 10^{17} - 10^{20}	10^{10} - 10^{13}	10^{5} - 10^{7}
Transmission E.M. Thin Foils 100kV foils <1μ 1000kV foils <5μ	Point ~20Å Fourier ~2Å	Clusters containing > 10^{2} defects 10^{12} - 10^{17}	10^{6} - 10^{11}	10^{3} - 10^{5}
Replicas		useful for extracting carbides in steels; also in fractographic analysis.		
Scanning E.M. metallographic methods surface observations	200Å	not applicable	possible in certain cases	10^{4} - 10^{5}
Special transmission scanning research microscopes	2-10Å	As for transmission		Depth of focus >1μ
X-ray topography in transmission 1 mm thick slices	0.1-1μ	Clusters containing > 10^{3} defects	1 - 10^{3}	1 - 10^{2}
			useful for non-metals, e.g. semiconductors	
Visible light careful metallography special etching	2000Å	generally not applicable	indirect 1 - 10^{8} if separated > resolving limit	1 - 10^{3} depth of focus ~ 2000Å

*This range indicates the lowest density consistent with a reasonable probability of finding that defect: the upper limit corresponds to that at which overlap and confusion occurs.

systems and in practice the effective aperture of an objective lens is $\sim 10^{-2}$ to 10^{-3} radians. This small value is used in order to minimize the four most important sources of error in the image: diffraction error, spherical aberration, astigmatism and chromatic aberration. As a result, even for electron wavelengths as small as 0.037Å (100Kv electrons), the optimum resolution in electron microscopy is insufficient for atomic resolution.* The only imaging system capable of resolving atoms is the field ion microscope. Table 1 summarizes the main matallographic techniques as applied to the resolution of lattice defects.

Although for many purposes a high power microscope is essential to the metallographer, some obvious structural features can be observed by eye or with the use of a low power hand lens. Such macrostructural details include cracks, porosity, segregation in castings, grain size, fracture characteristics and flow lines in forgings or extrusions, etc. The Magnaflux and Magnaglo processes are extremely useful for detecting small macroscopically invisible surface flaws which may be dangerous. In the former method magnetic particles are made to collect at discontinuities in the surface. For non-magnetic materials a dye containing oil is allowed to penetrate into the cracks (Magnaglo Process) and are visible under ultraviolet light because then the dye fluoresces. Various non-destructive techniques can also be used for detecting internal flaws, e.g. by ultrasonic testing.

Figure 2 shows an historical, but still beautiful micrograph, taken by Widmanstatten from a meteorite. Widmanstatten's name now adorns all microstructures in which precipitated phases are crystallographically related to the parent crystal.

---

* A. V. Crewe has claimed atomic resolution by scanning-transmission E.M.

The usefulness of the light microscope has been well demonstrated but many properties were not explained by what could be seen in this instrument. Indirect structural determinations were made using x-ray diffraction techniques and for example, Guinier and Preston in 1938 showed that age-hardening in aluminum alloys was due to precipitation of the, then, invisible zones rich in copper. The term substructure then became used to describe structure not resolved by the light microscope. The mechanical behavior of metals was explained qualitatively by the theory of dislocations as long ago as 1932, but dislocations were not resolved until quite recently when x-ray and electron microscopy techniques were developed. In the latest phases of metallography (fig. 1) the development of the field ion microscopy has now enabled the individual atom to be resolved.

It is the object of these lectures to describe generally but briefly the latest techniques which are available for direct structural observations. All I can do here is to hint at the type of work that is being done and the reader should not be misled by the brief and oversimplified descriptions. The reader should also become familiar with basic concepts of crystallography, optics and diffraction theory. The references given are typical but not exhaustive, since the literature describing each single technique and its applications is now voluminous.

2. Optical Metallography

For over 80 years, the light microscope has proved to be immensely valuable in understanding the structure of many materials but unfortunately since the best resolution obtainable is ~ 1100Å most of the important substructural features in metals, e.g., dislocations, small particles, etc., are not observable. Reviews of metallographic techniques for light microscopy are given in ref. 1.

Figure 3 shows the structure after deformation of a steel containing martensite and retained austenite (a) polished prior to deformation. After repolishing (b) the slip lines in the austenite have been removed but the deformation markings in the martensite remain. This simple but elegant demonstration shows that this type of martensite deforms by mechanical twinning. In low carbon steels, however, the martensite deforms by slip. Recent work using transmission electron microscopy has shown that in the former case the martensite contains very fine transformation twins not resolvable in the light microscope. This is an example where the combination of light and electron microscopy is extremely valuable in helping to understand complex phenomena.

The light microscope has been used to study dislocations in crystals by means of the etch pit technique. The development of the method owes much to the pioneering efforts of Vogel, et al.[2] who established a one-to-one correspondence between etch pits and dislocations in germanium. Regel et al.,[3] Johnston,[4] Forty[5] and Mitchell[6] have reviewed etch pitting techniques. Procedures and techniques are described in the former two references.[3,4] In the etch pit method it is necessary to find a chemical solution which preferentially attacks places at the surface where dislocations emerge. Often only certain crystallographic faces respond to the etchant.[7]

In metallurgical research considerable attention is being paid to the behavior of bcc metals in order to understand yielding behavior. Since it appears that the yield phenomenon is realted to the number and velocity of mobile dislocations[8] estimates of these numbers are needed. Table I gives a comparison of the methods whereby defect densities including dislocations can be estimated. The calssical etch-pit

experiments of Low et al.[9,10] demonstrated the velocity - stress dependence of dislocations in iron.

However, the etch pit technique suffers from the following difficulties: A count of dislocation etch pits in a slip band usually has no relation to the number of moving dislocations. This is because the pits denote immobile dislocations in the form of loops and dipoles. Also the density of pits has nothing to do with the shear strain in the slip band, since the latter is determined by the number of dislocations that have traversed the slip planes and left the crystal, and is not necessarily related to the debris left behind.

Although it was thought that etch pits could only be formed at dislocations which had impurities associated with them it is now believed that "clean" dislocations can also be revealed (see ref. 6). Decoration of dislocations by precipitates enables them to be observed in transparent crystals[7] and in metals by replication techniques.[11]

The etch-pit method is powerful, rapid and non-destructive. Dislocations can be revealed by applying stresses after etch pits have been formed and then located in their new positions by a further etch. The main limitations are knowing whether all pits always correspond to dislocations. The ability to produce dislocation etching depends critically upon the orientation and state of the specimen surface and on the precise composition of the etchant. Pits are not formed on low index faces which dissolve at the highest rates in a particular etchant, and the shape, resolution and size of pits depends on the nature and concentration of the controlling impurity, e.g., bromide ions for copper etches. If the density of dislocations is much above 10^8, interactions

between overlapping pits renders resolution of individual pits difficult if not impossible. Surface replication and examination in the electron microscope is helpful under these circumstances. Ideally combinations of the methods shown in Table I should be used on the same specimen if the most reliable information is to be obtained.

3. X-Ray Microscopy

Since x-rays have greater penetration into matter than either light or electrons, microstructural features can be investigated in opaque specimens. However, there are difficulties in making x-ray microscopes in that lenses for refracting x-rays are impractical.[12] Projection microscopes have been utilized for mostly biological work but some applications to segregation and alloy structures have been carried out.[13,14] Direct x-ray magnification is obtained by placing the sample close to the x-ray source and the photographic plate some distance away. For a magnification of 100x in a camera of length 10 cm. the sample is 1 mm. from the source. When the sample is placed next to the photographic plate contact microradiographs are obtained. In this case there is a 1:1 magnification. Both methods rely upon the relative absorption of x-rays from areas of the specimen containing different elements. Microgradiography and projection microscopy have been considered in books and reviews,[12-15,20] and further details and applications can be found in these references.

X-ray diffraction micrographs can be obtained which resolve substructure in materials, including individual dislocations. The technique has some advantages over electron microscopy and etch pit methods in that the specimen can be observed non-destructively and

without subject to damage although the defect density cannot be too high (Table 1). Also thick specimens can be studied. Two main techniques are employed, viz. the Berg-Barrett[16,17] and the Lang[18] methods. The former is simple and inexpensive whereas the latter requires more complex apparatus, thinner crystals and long exposure times for photography.

The principle of the two methods is shown in the sketches of fig. 4. The methods rely upon diffraction of x-rays whenever Bragg's law is satisfied. Since the images are formed of the diffracted beams they are dark field images. The Berg-Barrett method can be used for thicker crystals by taking reflecting photographs (fig. 4b) and both techniques (fig. 4a,c) are suitable for transmission work.[13,19-23]

Transmission Berg-Barrett

Parallel x-ray beams from a linear x-ray source are used so that a photograph of a given width of crystal can be obtained with only one exposure. An ordinary sealed-off x-ray tube is sufficient as the source. Since it is difficult to remove the K_{α_2} lines the resolution is limited by the dispersion of K_{α_1} and K_{α_2}. For example, when a focus of 1 mm. length horizontally and 0.5 mm. width vertically is used and the source-specimen distance is 50 cm., the specimen-plate distance is 1 cm., the resolution is 10μ and 7μ respectively in the normal and parallel directions using MoK_{α} reflected by (111) silicon.

Lang Method

As shown in fig. 4a if a point focus x-ray source (characteristic radiation) is used the K_{α_1} line only can be used to illuminate the specimen. After diffraction, the diffracted beams only reach the photographic plate (placed normal to the beam) since the transmitted

beam is stopped by the slit S_2. In order to obtain a projected image over a wide area of the specimen both the crystal and plate are simultaneously moved to the left and right. The images of each area are thus recorded continuously. In both techniques the images are magnified optically for observation. The resolution possible with this arrangement is ~0.5μ. In obtaining images of dislocations, the resolution of the camera should be ~1μ giving an image width of 10-50μ. For this reason investigations can only be carried out on crystals with a relatively low dislocation density ($10^8/cm^2$ or less). Figure 5 shows an example of dislocations generated in silicon as a result of indentation by a fine pointer at 1000°C. The reflection used is $\bar{1}\bar{1}1$.

As will be seen later (fig. 13) a defect whose displacement vector $\vec{R}$ lies parallel to the reflecting plane does not change the direction of the diffracted beam and so the defect is then invisible. Since the reciprocal lattice vector is normal to the reflecting plane the criterion for visibility is thus $\vec{g}.\vec{R} \neq 0$. Thus, by examining different reflections and noting that when $\vec{g}.\vec{R} \neq 0$ the direction of $\vec{R}$ can be determined.

Scanning Electron Microscopy[24,25]

The scanning electron microscope (SEM) is similar to the transmission electron microscope (TEM) but has these important differences: a) the image is of the surface and is formed as a result of excitations induced by the beam, e.g. secondary or reflected electrons, b) the voltage is much lower, 10-25 keV compared to the 100-1000kV power of the TEM, c) bulk samples rather than thin foils can be used, so sample preparation is much easier, d) the SEM uses

much lower beam currents ($\sim 10^{-10}$ amp) and so heating effects tend to be minimal, e) in the SEM the electron beam scans the sample whereas in the TEM the beam is stationary. However, both together make a powerful metallographic combination.

Figure 6 is a schematic diagram of a scanning microscope. The scan generator scans the electron beams in the microscope and in the cathode ray tube synchronously. Both beams trace out a raster, one on the specimen and the other on the CRT. As the beam hits the sample secondary electrons are excited which generally vary from point to point on the surface and so the brightness and contrast varies with the surface, e.g. at topographic differences, compositional differences, etc. The secondary electrons are collected and can be displayed by video signal on the CRT similarly to the principle of television. Specimens must be conductive so metals are ideal.

It should be emphasized that any signal generated by the incident beam at the surface of the sample will give rise to images, e.g. photons, back-scattered (reflected) electrons, induced currents in the sample, and so on. Differences in voltage can also be resolved and this makes the scanning microscope a powerful tool for analysing defects in semiconducting devices. For example, fig. 7 shows a SEM image of a commercial integrated circuit. All the junctions are visible and also the 2-volt drop across the collector resistor between C and R. This image was obtained after about 1 minute scanning following maximum resolution attainment.

Because of the enormous depth of field and focus that is available for electron images (due to the small wavelength) it is

possible to view very rough surfaces directly. Thus, a major application in metallurgy is fractography.[25] Figure 8 shows examples of ductile and intergranular tensile fractures in Cu-Ni-Fe alloy. Since sample preparation is quite minimal and as specimens can be observed directly, SEM is replacing the classical replica fractography techniques used in TEM.[30]

Undoubtedly the SEM is very versatile and a great improvement over visible light microscopes in terms of resolution and depth of field. Some minor disadvantages include long exposure times as compared to those for TEM, poorer resolution in reflection than TEM although the very latest techniques of scanning transmission microscopy have reportedly resulted in the resolution of heavy atoms in biological samples.* Very recent advances include the development of systems which allow dynamic experiments to be done, e.g. deformation, heating, cooling. Different types of information from the sample can be displayed on separate CRTS simultaneously. Characteristic x-ray emission can be monitored so the SEM can also be used as a microanalyzer.

In fairly perfect crystals patterns similar in appearance to Kikuchi patterns can be obtained (so-called pseudo-Kikuchi, channelling, or Coates patterns). It is possible, therefore, to obtain crystallographic information by SEM and to do selected area diffraction analysis although on a coarser scale than is possible by TEM.

In summary SEM is a very versatile surface metallographic technique and has been developing very rapidly in the past few years.

---

* A. V. Crewe, J. Wall and J. Langmore, Science 168, 1338, 1970.

Emission Electron Microscopy[26,27]

Figure 9 shows a schematic diagram of an electron emission microscope. It works in the same magnification and resolution ranges as SEM but the contrast mechanism is quite different; and it is most suited for metallographic studies of plane surfaces (compared to topographic applications by SEM). The principle is to excite electron emission from the specimen surface. In fig. 8 this is achieved by ultraviolet light bombardment. The specimen is kept at a negative potential and the electrons emitted from the surface are accelerated through the anode and are imaged in the electron optical system. The resolution is 150-300Å.

Since electron emission is determined by the work function for electrons, contrast is marked between areas of different compositions and orientations, and independently of any differences in topography. Electron emission microscopy is ideal for imaging at high temperatures because thermionic emission can occur so that dynamic studies can be followed directly. The highest vacuum must be obtained at the specimen in order to prevent oxidation. The following is a list of some applications of the technique:

1. Phase transformation, phase boundary-temperature relations
2. Recrystallization and grain growth
3. Cold work
4. Creep
5. Diffusion
6. Segregation
7. Solidification
8. Surface adsorption and other surface reactions
9. Electron emission; measurement of work function

Transmission Electron Microscopy

Replica Methods[28,29,30]

The earliest application of electron microscopy to metallurgical research involved surface replication.[31-35] The usual replicas now used are carbon or SiO, while for Al and its alloys their own oxide films can be used. The metal surface is covered with a replicating medium of 200-500Å thickness. In the case of C and SiO films these are produced by vacuum evaporation after the specimen has been prepared metallographically in the usual way. Oxide films on aluminum and its alloys are produced by anodising the surface. Second phase particles usually do not form a coherent oxide film so that holes at these regions in the replica delineate such particles. The replicas must be detached chemically from the metal by electrolytic polishing or etching. In the case of ferrous materials since precipitates are cathodic with respect to the matrix etching through the film allows particles to be extracted in the replica.[32] An example of extracted alloy carbide particles from a creep resistant steel is shown in fig. 10. These extracts can be examined by fluorescent analysis (e.g., by microprobe), in order to obtain information regarding their composition. Also since they are crystalline the selected area diffraction technique may be used to distinguish between the various phases which may be present, as well as to obtain structural information.

The maximum resolution possible with replicas is ~ 20Å. The replica technique has been widely used to study surface features associated with slip, precipitation phenomena, fracture, (see, e.g. refs.). However, with the advent of thin foil techniques in TEM

and scanning electron microscopy, replica methods are now being superseded.

Thin Foils[28,29,36-43]

Transmission electron microscopy of thin foils is now very widely used in metallurgy. The tremendously rapid growth of the method over the past decade is mainly due to:

(1) Development of techniques for preparing specimens thin enough to be transparent to electrons. The useful transparency thickness increases with voltage as shown in fig. 11a.

(2) The availability of electron microscopes with double condenser lens systems, selected area diffraction and high voltage facilities. (now up to 1 meV and 3 meV). See fig. 11(b).

(3) Development and application of the theory of electron diffraction which facilitates the interpretation of the often complex images observed.

(4) The extensive information retrieval that is now possible in one instrument (fig. 12).

The electron microscope image is a projection at magnifications of 10^2 - 2×10^5 of the volume of the foil through which the electron beam is passed. The resulting picture is thus a two-dimensional projection of the three dimensional object. However, the three-dimensional character of the object is obtained by stereomicroscopy where two views of the same area, tilted by about 10°, and under the same contrast conditions, are obtained.* Point resolutions of about 20Å can be obtained and Fourier resolutions of ~ 2Å have

* See figure 14 of the chapter on non-equilibrium microstructures.

been achieved.

There are many complex interactions which occur when electrons travel through crystals. The most important of these is diffraction since this is the major phenomenon giving rise to contrast in the image. The interpretation of contrast phenomena thus depends entirely on the theory of diffraction. This theory has now been developed to account for unusual effects associated with absorption and provides extremely useful and detailed information. Because of the small wavelength of electrons the diffraction angles are very small ($\sim 10^{-2}$ rad.) so that only planes which are approximately normal to the foil surface will diffract.

In order to accomplish direct lattice resolution, the transmitted and diffracted beams must combine at the image plane. Hence, the angle 2θ between these beams must be less than the effective aperture of the objective lens. In order to minimize aberrations the lens aperture α_o is $\sim 10^{-2}$ radian. Hence the resolution limit is $\sim \lambda/2\,\alpha_o$. For 100 kV electrons $\lambda = 0.037\text{Å}$, hence the minimum resolvable spacing is about 2Å and low index planes in metals and semiconductors have now been resolved. Indirect resolution is possible by means of moiré images.

With metallurgical specimens, contrast is generally obtained by <u>not</u> allowing the transmitted or diffracted beams to contribute to the image. This is accomplished by the use of 30μ apertures in the back focal plane of the objective lens. (fig. 13). If all diffracted beams are excluded, a bright field image is thus formed. The dark field image is obtained by allowing a single diffracted beam to reach the image plane. With the facilities for selected area diffraction, detailed information regarding substructure can be obtained and the dark field technique is an

invaluable aid in identifying microstructural features.

Perturbations in the lattice such as are caused by defects lead to perturbations in the scattered beams compared to the scattering occurring in the perfect lattice. This difference in scattering may be manifested as changes in phase, amplitude or both. A particularly simple visibility criterion holds true for lattice defects as can be seen by considering Bragg's law: Sin $\theta = n\lambda/2d$ where d is the spacing of the reflecting plane, θ is the Bragg angle and λ the wavelength. $(d^{-1}) = |g|$ in the reciprocal lattice. If displacements R in the lattice do not alter d (or $|g|$) then sin θ is unaltered and no phase contrast can occur. Stated in vector terminology $\bar{g}.\bar{R} = 0$ is the invisibility criterion. Thus images of the same defect taken in different diffraction vectors enables the direction of $\bar{R}$ to be found e.g. figs. 14, 15, 18. Actually, contrast is adequate only when $\bar{g}.\bar{R} > 1/3$ so that unless high order reflections are used partial dislocations of small Burgers vector (e.g. the a/6<111> twinning dislocation in bcc metals) may never be visible. Although the visibility increases with $\bar{g}$, the resolution worsens. Image analysis requires an adequate knowledge of crystallography and diffraction theory.

It is almost standard procedure now to utilize computer programs for contrast analysis and interpretation. Recent innovations include (e.g. ref. 23) computer simulation of the image, i.e. the computer prints out simulated images which can be compared directly to the observed (provided both match in terms of diffraction conditions, foil thickness, etc.). An example is shown in fig. 16. One of the few limitations today is the ability to analyze in detail alloy structures containing large volume fractions of small defects, e.g. G.P. zones, fig. 17, ordered alloys,

fig. 18, because the strain field overlap and become complex. Similar difficulties exist for heavily irradiated metals containing large numbers of vacancy/interstitial defects. At high voltages many beam scattering events occur and the theory must be modified to account for these interactions.

Selected area diffraction is an important advantage of electron microscopy and this feature is unique. With crystalline objects a diffraction pattern is formed at the back focal plane of the objective lens. This pattern which can be selected from a given area (minimum 2μ dia at 100kV, but 0.02μ at 1000kV) can be magnified onto the fluorescent screen and rapid examination of the image and its diffraction pattern is routine. Kikuchi diffraction patterns are particularly valuable.(e.g. ref.23,40) Interpretation of the image and its diffraction pattern is facilitated by dark field analysis of the diffracted beams. High resolution dark field images are obtained by tilting the illumination such that the diffracted beam passes down the optical axis. Contrast is enhanced by allowing only this beam to pass into the imaging system.

The list of applications of TEM is almost limitless but major applications in metallurgy/materials science involve characterization of the structure of materials and the relation between structure and properties. The characterization includes:

a) Observation and identification of lattice defects (dislocations, stacking faults, small defect clusters, precipitates, etc.

b) Crystallographic data from electron diffraction.

c) Surface investigations, replication, reflection and scanning microseopy; fractography.

d) Qualitative chemical analysis of characteristic x-rays emitted by the foil.

e) Energy analyses for contrast and for identifying elements (by scanning microscopy also).

f) In situ investigations of crystal growth, epitaxy.

g) Examination of specimens at different temperatures; deformation, bombardment in situ.

Future applications will resolve around extending the range of materials to be analyzed particularly by high voltage electron microscopy,[26,40,44-46] e.g. ceramics for which specimen preparation is difficult although ion thinning techniques are very promising, and polymers which suffer seriously from ionization damage at accelerating voltages below about 300kV (the ionization scattering cross sections decrease with increasing energy). The question of damage is an important one: in metals it is possible to produce primary knock-on events once the threshhold energy is exceeded (e.g. 500kV for electrons in copper) so that direct studies of electron irradiation are possible. Conversely one does not wish to have radiation events occurring which might produce spurious effects in the structures under study.

Energy Analyzing and Energy Selecting Electron Microscopy[40,47]

In addition to the elastic scattering that is responsible for Bragg diffraction of electrons, electrons can lose energy as a result of inelastic scattering processes involving excitations such as phonons, plasmons, ionization, etc. The specimen is likewise excited into a higher energy condition and in principle the energy levels in solids can be studies by measuring the energy loss spectra of the

incident electrons. Since compositional changes also involve energy level changes, the loss spectra should be characteristic of composition.

The difficulties of carrying out these measurements stem from the small range of energy losses, e.g. the plasmon loss for metals is in the range 10-50eV (15eV for Al). Two types of instruments have been developed, the energy selection and energy analyzing microscopes. These utilize in different ways the information that is contained in the loss spectra of electrons which form the image. In the energy analyzing microscope a fine slit is placed in the final image plane. This slit is made the entrance aperture of an electron spectrometer - such as a lens, which can spread the loss electrons in a direction normal to the slit by amounts determined by the dispersion of the analyzer. The displacement Δ which can be recorded on film and measured, is given by $\Delta \simeq C_c \alpha \Delta E/E$ where C_c is the chromatic constant of the lens, α the scattering angle, E the incident electron energy and ΔE the energy loss.

In the energy selecting microscope the electrons forming the image are initially dispersed into their loss components by an analyzer and by using apertures and subsequent focussing or scanning systems one of the energy loss components is collected to form the image.

The energy analyzing microscope can be used either in diffraction or imaging modes and measurements of the loss spectra can be made in analyzing compositional variations in alloys, provided the loss spectra of the elemental components are well defined and easily distinguisable. Good success has been obtained in Al-Mg alloys (plasmon loss in Al = 15.3eV and in Mg = 10.4eV). For simple plasmon excitation the energy

loss is directly proportional to the number of free electrons/unit volume. The spatial resolution limit is ~ 100Å.

These techniques are relatively new but offer much promise for microanalysis in the electron microscope. A detailed acount is given by Metherell.[47]

Field Ion Microscopy[29,48]

The field ion microscope is the only instrument capable of atomic resolution and was developed by Müller from his earlier field-electron (emission) microscope.[49,50] In its simplest form the microscope consists of a metallic specimen, which is a very fine wire sharply pointed to a tip radius of ~ 300 atoms, as anode placed opposite a fluorescent screen at ground potential and both mounted in a highly evacuated glass (or metal) tube. The potential applied to the tip is ~ 500 mV/cm which is sufficient to allow field ionization of the imaging gas which is usually helium. This gas is introduced at a pressure of a few millitorr, low enough to allow the ions to reach the screen without interference collisions. The tip is usually cooled cryogenically to increase resolution by decreasing thermal vibrations in the specimen. The development of flat screens and fiber optics allows weak images to be photographed. Firgure 19 shows schematically a field ion microscope as used for direct studies of radiation damage (Petroff and Washburn[51])

The potential is chosen so as to allow ionization to occur only at the surface atoms without field evaporation also taking place. The latter is determined by the cohesive strength of the specimen and initally only the refractory metals could be imaged under the

conditions needed to form the ion images. However, with gases of lower ionization potentials, e.g. Ne, H_2, and image intensification techniques, a much wider range of metals becomes possible. With small tip radii magnifications of 10^6 are easily obtained. Metallurgical applications of this technique include basic studies of lattice defects, by taking advantage of atomic resolution, surface diffusion, in situ experiments such as cathode sputtering, irradiation damage (fig. 20), early stages of precipitation in iron and nickel base alloys,[52] cyclic field stressing simulating fatigue deformation, in situ surface changes after successive field evaporation (facilitated by color printing) observations of interfaces, particularly the successful analysis of grain boundaries[52,53] studies of alloys, especially ordering (fig. 21). One of the current limitations is not one of technique, but rather of interpretation; e.g. difficulties in interpreting point defects, particularly interstitial atom images, and alloy systems in which images are irregular (fig. 21b). When used in conjunction with other techniques some of these difficulties can be overcome. The interpretation of FIM images is facilitated by applying computer simulation techniques. The basic criteria adopted rely upon the imaging characteristics the most important of which are a) the tip is hemispherical, b) only atoms lying within a very small distance of the surface contribute to imaging, c) the planar poles in the image are arranged as in stereographic projections[54] d) field evaporation preferentially removes atoms of lowest binding energy and atoms are imaged only if it is field evaporated at potentials above those required for ionization of the imaging gas.

One of the most significant advances in FIM in recent years is the development of the atom probe by which atomic mass spectrography can be accomplished.[55]

The principle of the method is to field pulse evaporate, at a potential V_p, a selected atom which has been imaged at the voltage V through a hole in the observation screen. The atom travels down a tube length ℓ to a detector and the time of flight t is related to its kinetic energy from which the mass M is derived from the relation $M = 2ne(V_o + V_p)t^2/\ell^2$ where ne is the total ionic charge. The mass resolution claimed for this device is $\Delta M/M = 1/250$. Calibration of the instrument is usually done by imaging known metals and obtaining time signals for known masses.

X-Ray Microanalyser (Microprobe)[13,56]

This method is particularly useful for general chemical analysis and identification of inclusions, segregation, etc. at spatial resolutions ~1μ and impurity detections of ~ 10^{19} atoms/cm^3. The microprobe uses a scanning electron beam to generate characteristic x-rays in the specimen. The x-rays are examined in x-ray spectrometers so that intensities can be determined of the characteristic lines. The secondary electrons can also be imaged on CRTs and the surface topography obtained and compared with the x-ray distribution which can also be selectively displayed by utilizing each characteristic line in turn. Figure 22 shows an example of segregation analysis across grain boundaries (compare to fig. 8).

The limitations are in resolution and the x-ray spectrometer. In order to anayse over the whole range of atomic numbers a series

of selecting diffracting crystals is needed. Since the efficiency of scattering and detectability both decrease with decreasing atomic number considerable difficulties exist for analysing light elements $Z < 10$.

In steels it is not yet possible to distinguish carbides from nitrides when present in small quantities.

Kossel-Lines[22,58]

Since the probe provides a fine focus electron beam, a specimen can be used as a target for producing a divergent x-ray diffraction pattern. A single crystal gives a large number of light and dark lines called Kossel lines from which the most accurate determinations of lattice parameter can be made. In order to avoid electron transmission and to produce optimum x-ray diffraction, the thickness of the specimen must be ~ .004 to .01 ins.

Kossel patterns can also be obtained using a micro-focus x-ray tube. This technique can be readily combined with projection x-ray microscopy since the specimen position is the same in both methods.[22]

Besides the advantages of obtaining very accurate lattice parameter measurements and orientations the technique is a sensitive one for studying crystal perfection, e.g. for strained materials the Kossel lines are split. From measurements of the fragmentation information regarding internal strains in the material can be obtained.

Summary

The metallographic techniques described above fall into two categories: a) studies of surface structure and composition by methods of light microscopy, electron microscopy (scanning, electron emission, replicas) and field

ion microscopy and b) studies of bulk or internal structure and composition by x-rays, transmission electron microscopy and field ion microscopy. These techniques have been developed extensively over the past 80 years and are summarized in fig. 1..

Indirect methods of examining structure rely either on diffraction effects and their interpretation, or rely on measurements of a parameter which is structure sensitive, e.g. electrical conductivity, internal friction, resonance techniques, and so on. The main indirect diffraction methods include x-ray and neutron diffraction (electron diffraction is included in the "direct" electron microscopy category), surface electron diffraction either at low energy (L.E.E.D.) or high energy (H.E.E.D.). These methods will not be discussed further here, but information about them can be found in reference 59.

References*

1. R. Fichter, S. Arch. Wiss und Tech., 28, 235 (1962).
2. F. L. Vogel, W. A. Pfann, H. E. Corey and E. E. Thomas, Phys. Rev., 90, 489 (1953).
3. V. R. Regel, A. A. Unusovakaya and V. N. Kolomiichuk, Kristall., 4, 937 (1959).
4. W. G. Johnston, Prog. Ceram. Sci., 2, 1 (1961).
5. A. J. Forty, Adv. in Phys., 3, 1 (1954).
6. J. W. Mitchell, Direct Observations of Imperfections in Crystals, Interscience, New York, 1962, p. 3.
7. W. J. Dash, J. Appl. Phys. 27, 1193 (1956); Dislocations and Mech. Prop. of Crystals, John Wiley & Sons, New York, 1957, p. 57.
8. See, e.g. G. T. Hahn, Acta Met., 10, 727 (1962).
9. J. R. Low and R. W. Guard, Acta Met., 7, 171 (1959).
10. D. F. Stein and J. R. Low, J. Appl. Phys., 31, 362 (1960).
11. G. Thomas and J. Nutting, Mechanism of Phase Transformations in Metals, Inst. Metals Mon #18, 57 (1956).
12. V. E. Cosslett, Met. Reviews (Inst. Metals London), 5, 225 (1960).
13. X-Ray Microscopy and Microanalysis, Elsevier Amsterdam, 1960.
14. X-Ray Microscopy and Radiography, Academic Press, New York, 1957.
15. J. J. Trillat, Met. Rev., 1, 3 (1956).
16. W. F. Berg, Z. Krist., 89, 286 (1934).
17. J. B. Cohen, Diffraction Methods in Materials Science, MacMillan New York, 1966.

---

* General up-to-date and comprehensive reviews appear in a series of books on Techniques in Metals Research by J. Wiley (N.Y.) edited by R. F. Bunshah. Volume II Part I covers much of the material presented here in great detail.

18. R. H. Condit, Techniques of Metals Research II, 877, 1969.

19. S. Weissman and Z. H. Kalman, ibid., p. 839.

20. P. S. Onj, ibid., p. 159.

21. Advances in X-ray Analysis, vol. 10, Plenum Press, New York 1967.

22. J. Auleytner, X-ray Methods for Study of Defects in Single Crystals, Pergamon Press 1967.

23. Modern Diffraction and Imaging Techniques in Material Science, Eds. S. Amelinckx, R. Gevers, G. Remaut, J. Van Landuyt, North-Holland Publ., Amsterdam, 1970.

24. P. R. Thornton, Scanning Electron Microscopy, Chapman & Hall, 1968.

25. Proceedings ITRI Conferences on Scanning Electron Microscopy, Chicago annually from 1968.

26. See the Proceedings of Electron Microscopy Congresses, e.g. Kyoto 1966, Rome 1968, Grenoble 1970.

27. L. Wegmann, X-ray Optics and Microanalysis, Tubingen, 1968, p. 345.

28. G. Thomas, Transmission Electron Microscopy of Metals, J. Wiley, New York, 1962.

29. D. G. Brandon, Modern Techniques in Metallography, Butterworths, 1966.

30. Electron Fractography, ASTM Publication #436, 1968.

31. ASTM Special Technical Publications (a) #155 (1953), (b) #245 (1958), and (c) #262 (1959).

32. R. M. Fisher, J. Appl. Phys., 24, 113 (1953). See also Ref. 41(a), p. 49.

33. Proc. 3rd Int. Conf. Electron Microscope, London (Roy. Mic. Soc.) 1956.

34. Proc. 4th Int. Conf. Electron Microscope, Berlin (Springer-Verlag) 1960.

35. Inst. Metals Rep. and Mon. series #8, 1950, Metallurgical Applications of the Electron Microscope.

36. Proc. 5th Int. Conf. Electron Microscopy, Philadelphia (Academic Press) 1962.

37. Electron Microscopy and Strength of Crystals, Eds. G. Thomas & J. Washburn, Interscience, 1963.

38. P. B. Hirsch, A. Howie and M. J. Whelan, Phil. Trans. Roy. Soc., A 252, 499 (1962).

39. R. D. Heidenreich, Fundamentals of Transmission Electron Microscopy, J. Wiley, 1964.

40. P. B. Hirsch, et al., Electron Microscopy of Thin Crystals, Butterworths, 1965.

41. J. W. Menter, Adv. in Physics, 7, 299 (1958).

42. A. Howie, Met. Reviews (Inst. Metals, London), 6, 467 (1961).

43. G. Thomas, Symposium on "Thin Films," ASM 1964, p. 227.

44. V. E. Cosslett, Contemporary Physics, 1968, 9, 333.

45. Micron, January 1970.

46. G. Thomas, Phil. Mag. 17, 1097 (1968).

47. A. J. F. Metherell, Adv. Optical, Electron Microscopy, 4, 1970, in press.

48. J. J. Hren and S. Ranganathan, Field Ion Microscopy, Plenum Press, 1968.

49. E. W. Müller, Z. Physik, 106, 541 (1937).

50. E. W. Müller, Z. Physik, 131, 136 (1951).

51. P. Petroff and J. Washburn, Rev. Sci. Instr., 39, 317 (1968).

52. D. M. Schwartz, A. T. Davenport and B. Ralph, Phil. Mag. 18, 431, (1968).

53. D. G. Brandon, B. Ralph, S. Ranganathan and M. Wald, Acta Met. 12, 813 (1964).

54. O. Johari and G. Thomas, Stereographic Projection and Applications, J. Wiley, 1969.

55. E. W. Müller, J. A. Pavitz and S. B. McLane, Rev. Sci. Instr. 39, 89, (1968).

56. Electron Probe Microanalysis, J. Inst. Metals, 91, 1962/63.

57. Advances in X-ray Analysis, Plenum Press (annually).

58. K. Lowsdale, Phil. Trans. Roy. Soc. 240, 219, 1947.

59. Structure and Chemistry of Solid Surfaces, Ed. G. Somorjai, J. Wiley, 1969.

Figure Captions

Fig. 1. Showing the development of the major imaging metallographic techniques for resolution of structure. X-ray topography is another method.

Fig. 2. Actual size meteorite polished and etched to reveal Widmanstatten $\alpha + \gamma$ microstructure[after Widmanstatten].

Fig. 3. Illustrating how light optical microscopy provides information on deformation modes. Fe-28Ni-0.45C steel partially transformed to martensite. After polishing and etching it was deformed in compression and photographed (a). In (b) the same area is shown after re-polishing. The lines in austenite in (a) are now removed but those in martensite remain. This shows the austenite deforms by slip and the martensite by twinning. Courtesy R. Munson and D. Schmatz, Ford Motor Co.

Fig. 4. Schematic diagrams illustrating the experimental arrangements for x-ray diffraction micrography (a) Lang method, (b) Reflection Berg-Barrett, (c) Transmission Berg-Barrett.

Fig. 5. X-ray topograph of dislocations in silicon. These were generated by indentation at 1025°C for 15 mins. Courtesy V. C. Kannan.

Fig. 6. Schematic diagram showing the scanning electron microscope. Courtesy T. Everhart.

Fig. 7. Scanning micrograph showing voltage contrast from an integrated circuit. The voltage drop C-R is 2 volts. Arrows show imperfections at the isolation junctions. Courtesy T. Everhart.

Fig. 8. Scanning micrographs showing topographic contrast of fracture surfaces in Cu/27Ni/9Fe spinodal alloy quenched a) then aged at 625°C for b) 1 min., c) 0.1 hr., d) 1 hr. showing abrupt change

from transgranular ductile (dimple) fracture to intergranular failure after 0.1 hr. aging. Notice large depth of field.

Fig. 9. Schematic diagram of emission electron microscope. Electrons are emitted from the specimen by heating (thermionic emission) or U.V. radiation (photoemission) and are focussed and magnified by the magnetic lens system.

Fig. 10. Carbon extraction replica of complex alloy steel. The carbides can be identified by electron diffraction; the very large ones are NbC (undissolved), the needles are $Fe_3 (MoW)_2$, small cubes of $(Cr\ Fe\ Mo\ W)_{23}C_6$ and very fine precipitates (on dislocations) of NbC. Courtesy M. J. Arrowsmith.

Fig. 11a. Showing the voltage-thickness dependence for high resolution transmission electron microscopy of silicon and stainless steel. The transmission decreases rapidly with increasing atomic number. Courtesy Phil. Mag. ref 46.

Fig. 11b. The Berkeley 650kV electron microscope showing the column, controls, and high voltage tank at the upper level. During operation the instrument is constantly monitored for possible X-radiation emission.

Fig. 12. Schematic diagram showing the main uses of and possible information retrieval from transmission electron microscopy.

Fig. 13. Illustrating Bragg's Law of diffraction and the reflecting sphere construction for electron transmission. Notice that displacements $\vec{R}$ in the reflecting plane produce no phase contrast.

Fig. 14. Illustrating the $\bar{g}.\bar{b}$ contrast criterion for dislocation contrast. Thin foil of Ag_2Al deformed 35% at 210°K. The

orientation is shown by the Kikuchi pattern in (c) to be near $[0\bar{1}13]$. In (b) the foil is tilted to $\bar{g} = 20\bar{2}1$ and in (a) $g = 2\bar{1}\bar{1}0$ as shown in (c). The loops thus have Burgers vectors of $1/3\langle 11\bar{2}0\rangle$ type.

Fig. 15. Interfacial dislocations in the partially coherent stage of spinodal decomposition in Fe/52Cu/33Ni aged 200 hr. 775°C. All three sets of dislocations can be revealed individually by using the different reflections indicated. This shows the Burgers vectors are $a/2\langle 110\rangle$ type.

Fig. 16. Stacking fault images in silicon for a foil give extinction distances thick (two-beam g = 220). The upper figure is the computer simulated image; the lower is the actual micrographs.

Fig. 17. Al-4%Cu thin foil dark field image showing strain contrast images for θ" and larger θ' particles. No zones are visible on (010) since for these $\vec{g}.\vec{R} = 0$. Orientation [001].

Fig. 18. Ni_4Mo aged 5 mins. at 750°C.

a) Diffraction pattern in [121] orientation showing superlattice reflections.

b) Dark field of $1\bar{1}0$ bct superlattice spot which images domains of one orientation - Structure Factor Contrast

c)-g) shows strain contrast images in the matrix reflections 002, $1\bar{1}1$, $\bar{1}11$ and $\bar{2}20$ respectively in a [110] foil. The contrast is due to many small microdomains having coherency strain fields.

Fig. 19. Schematic diagram of stainless steel field ion microscope designed at Berkeley for direct studies of radiation damage in the cyclotron. Courtes P. Petroff.

Fig. 20. Iridium single crystal before and after "field on" irradiation with 10 MeV protons at -196°C. (a) is before, (b) after irradiation. Dotted atoms in (a) have been ejected from the surface during irradiation and are missing in (b). Extensively damaged regions are indicated by arrows. Dotted atoms in (b) are surface interstitials and are missing in (a). The beam direction is indicated by black arrows. The difference between (a) and (b) is not an artifact, but a change in the overall contrast due to a change in the surface structure upon irradiation. Courtesy P. Petroff.

Fig. 21. (a) Regular images in ordered Ni_4Mo aged 125 hr. at 750°C. Disordered alloys do not have this regularity as shown in (b) which is as quenched.

Fig. 22. Microprobe analysis showing segregation at grain boundaries in alloy of 64% Cu - 27% Ni - 9% Fe aged 1000 hours at 625°C showing grain boundary segregation. Compare to fig. 8(d).

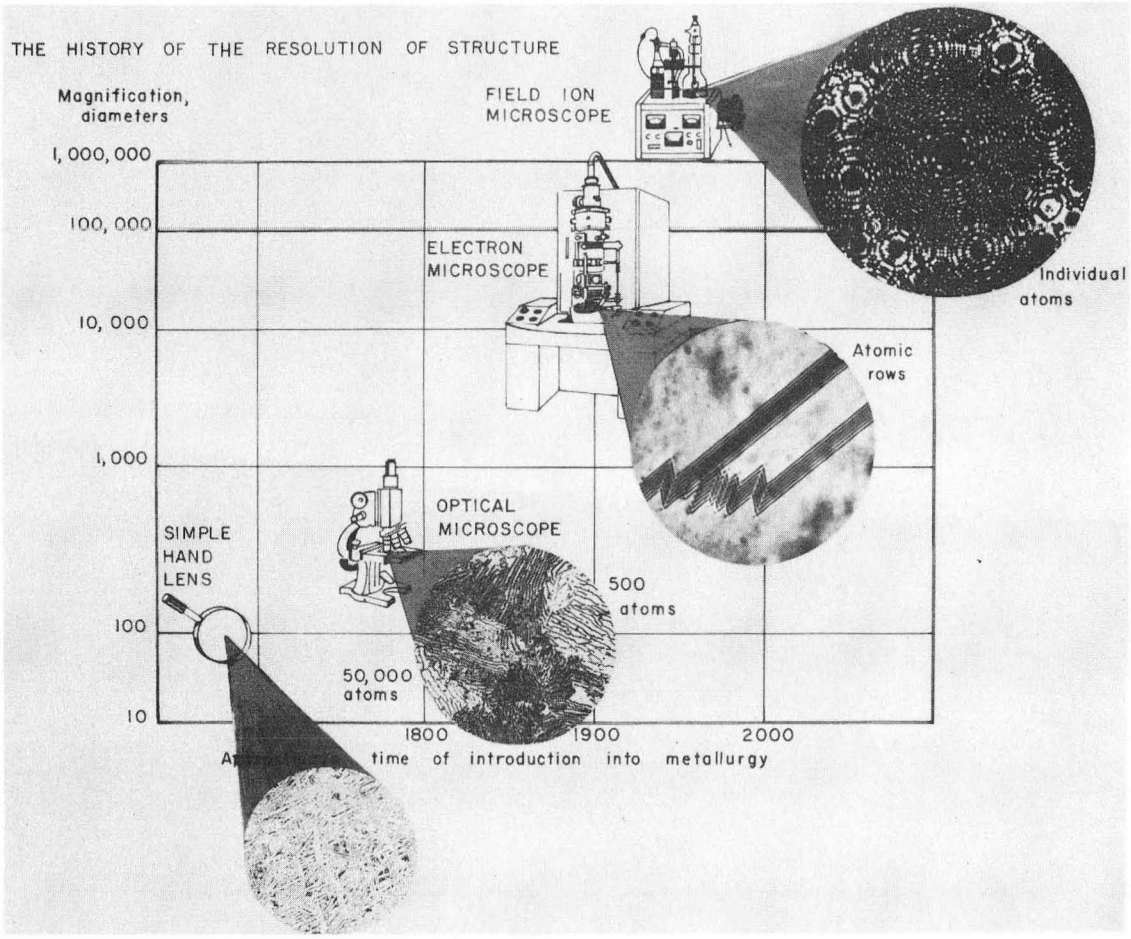
THE HISTORY OF THE RESOLUTION OF STRUCTURE
Magnification, diameters
1, 000, 000
100, 000
10, 000
1, 000
100
10
FIELD ION MICROSCOPE
ELECTRON MICROSCOPE
OPTICAL MICROSCOPE
SIMPLE HAND LENS
Individual atoms
Atomic rows
500 atoms
50, 000 atoms
1800
1900
2000
time of introduction into metallurgy

IM1982

Fig. 1.

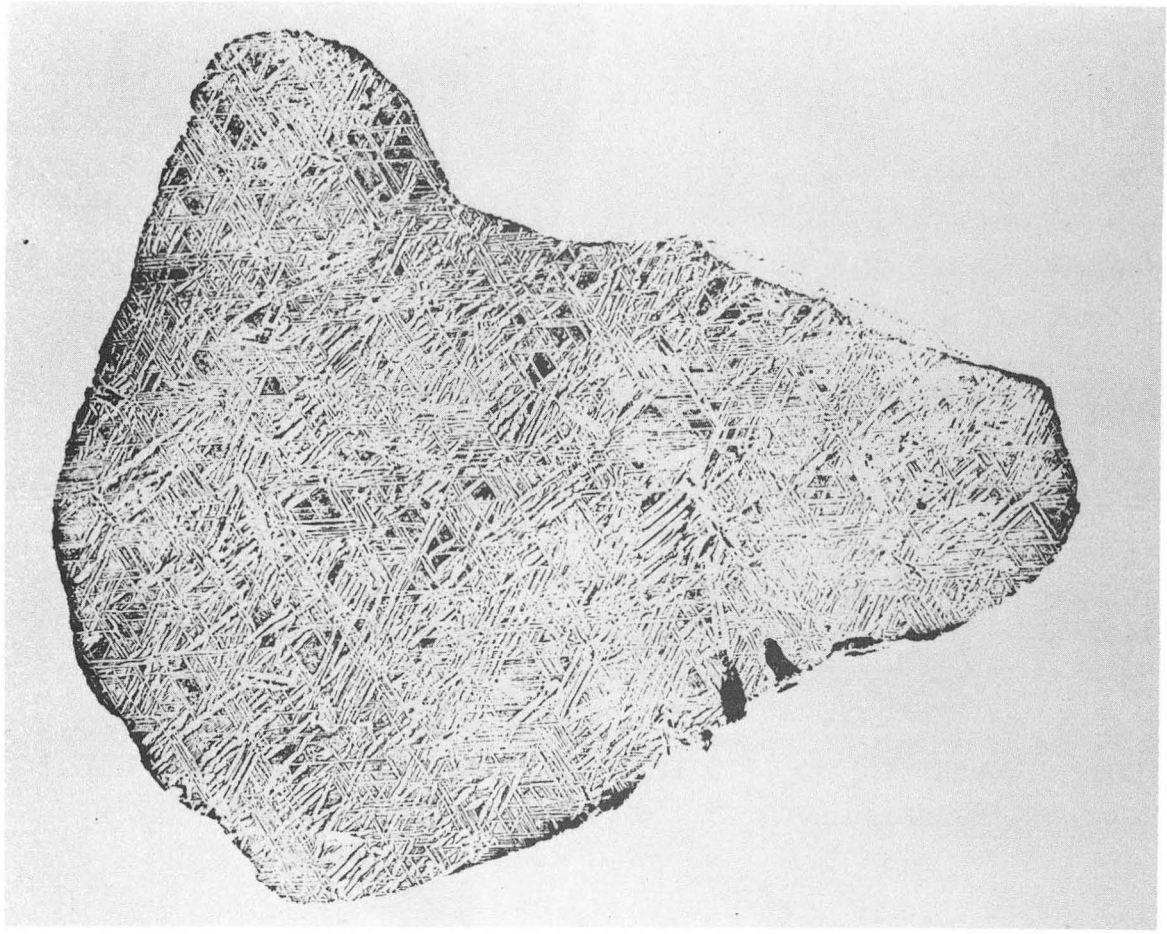

IM860

Fig. 2.

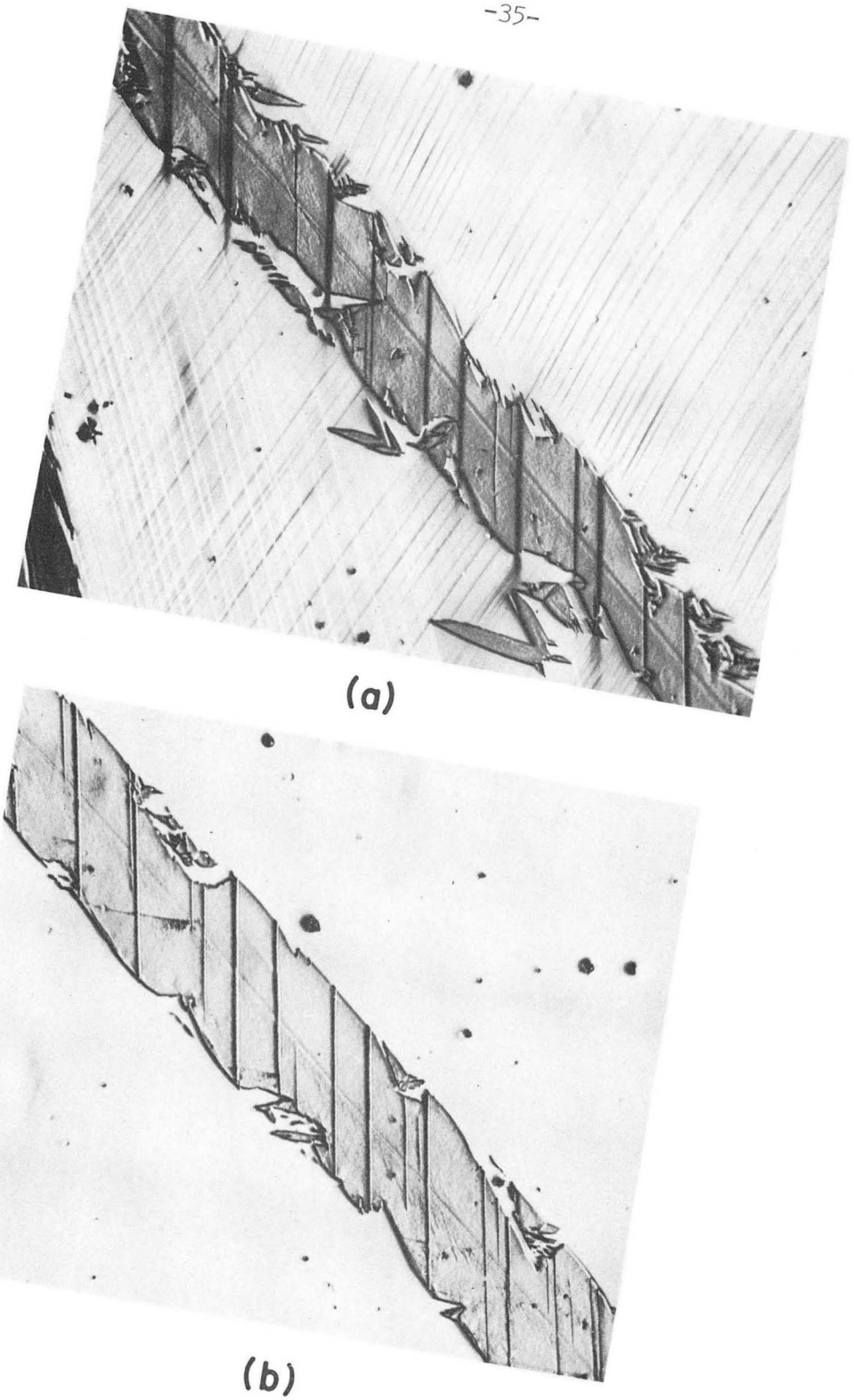

Fig. 3.

IM861

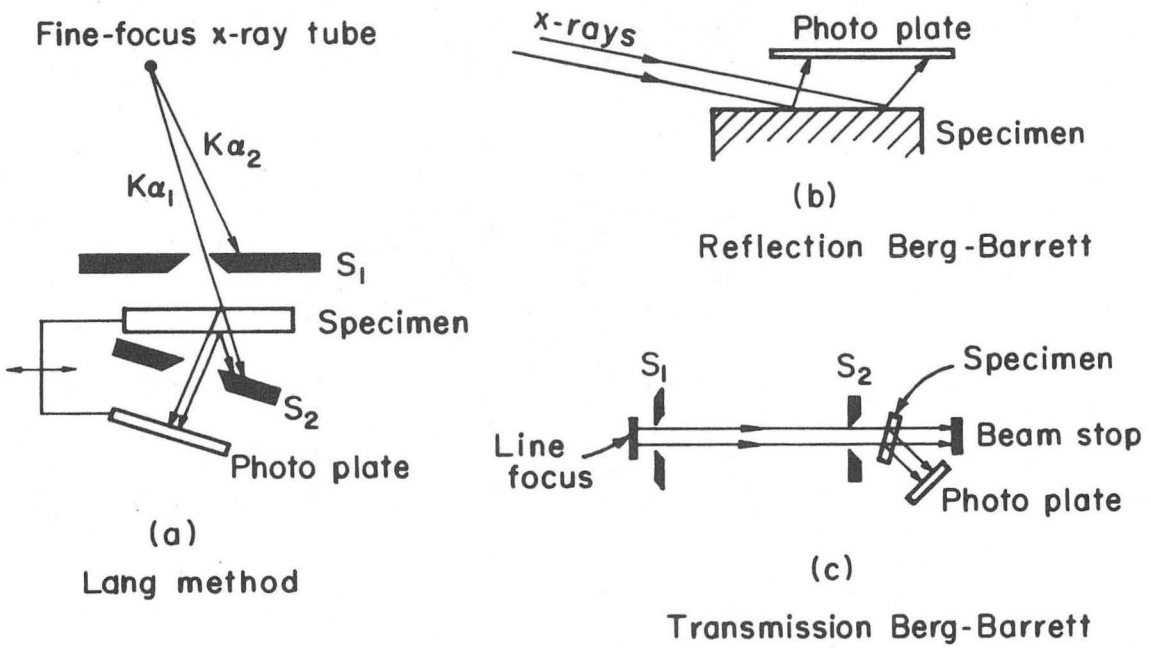
Fine-focus x-ray tube
Kα2
Kα1
S1
Specimen
S2
Photo plate
(a)
Lang method
x-rays
Photo plate
Specimen
(b)
Reflection Berg-Barrett
S1
S2
Specimen
Line focus
Beam stop
Photo plate
(c)
Transmission Berg-Barrett
MU-32482

Fig. 4.

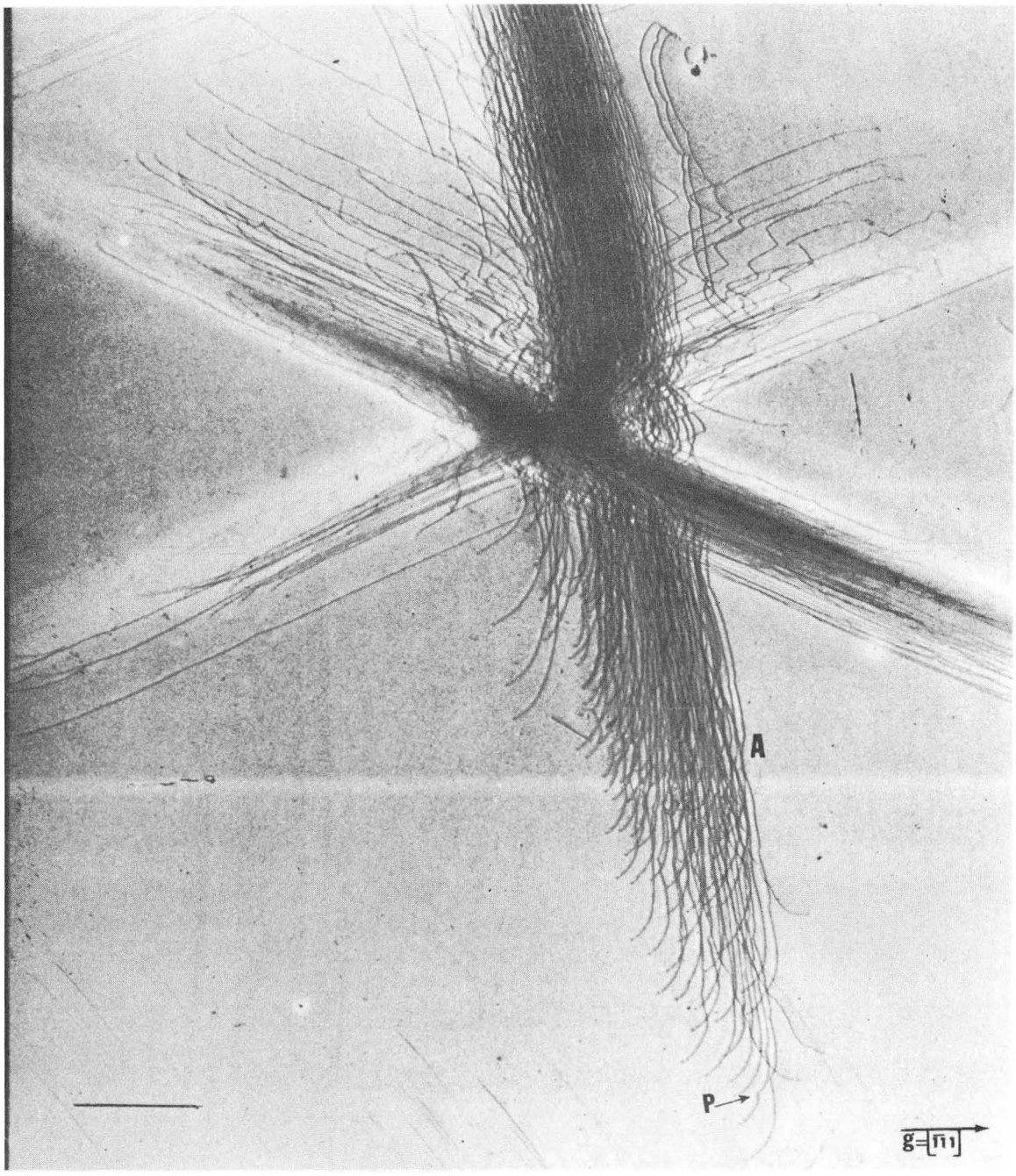

XBB6810-7421

Fig. 5.

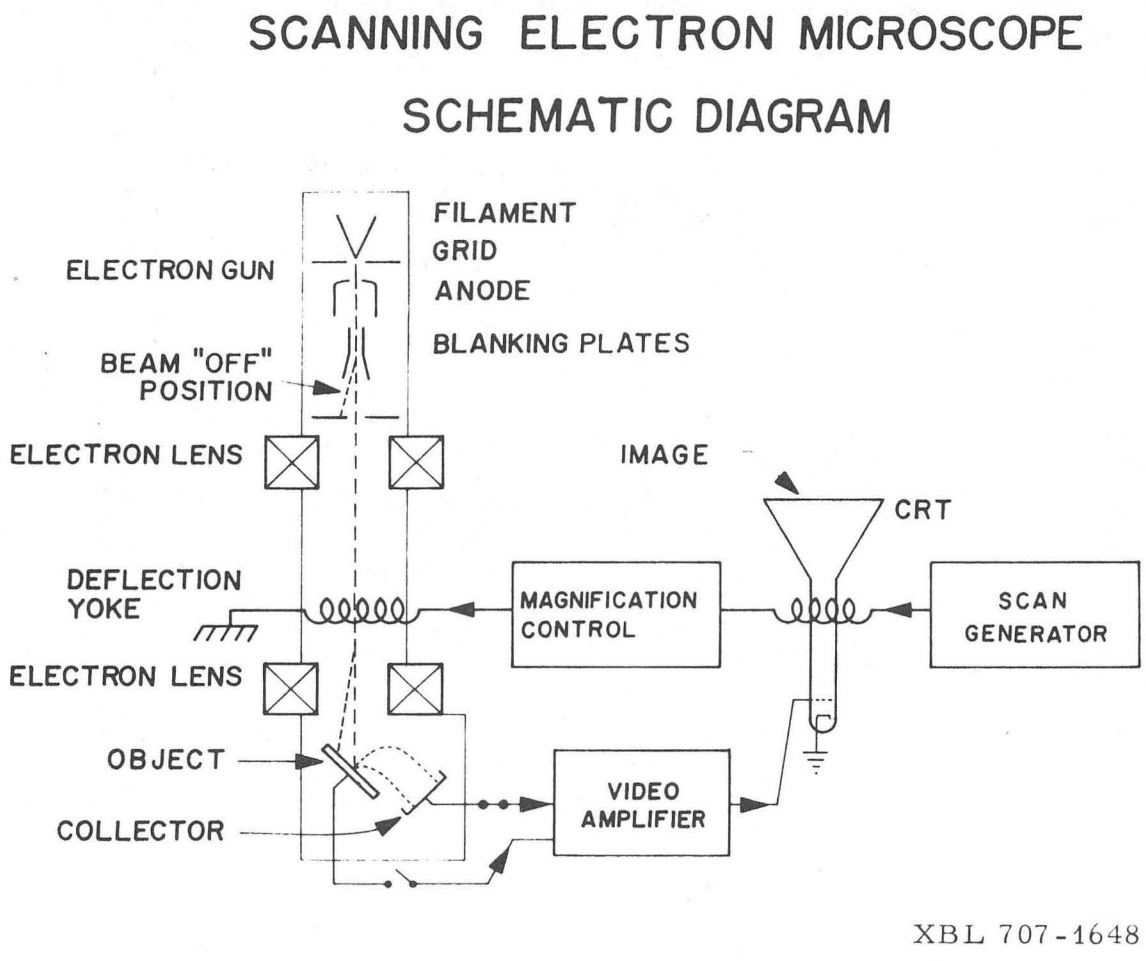
SCANNING ELECTRON MICROSCOPE
SCHEMATIC DIAGRAM
FILAMENT
GRID
ANODE
ELECTRON GUN
BLANKING PLATES
BEAM "OFF" POSITION
ELECTRON LENS
IMAGE
CRT
DEFLECTION YOKE
MAGNIFICATION CONTROL
SCAN GENERATOR
ELECTRON LENS
OBJECT
VIDEO AMPLIFIER
COLLECTOR
XBL 707-1648

Fig. 6.

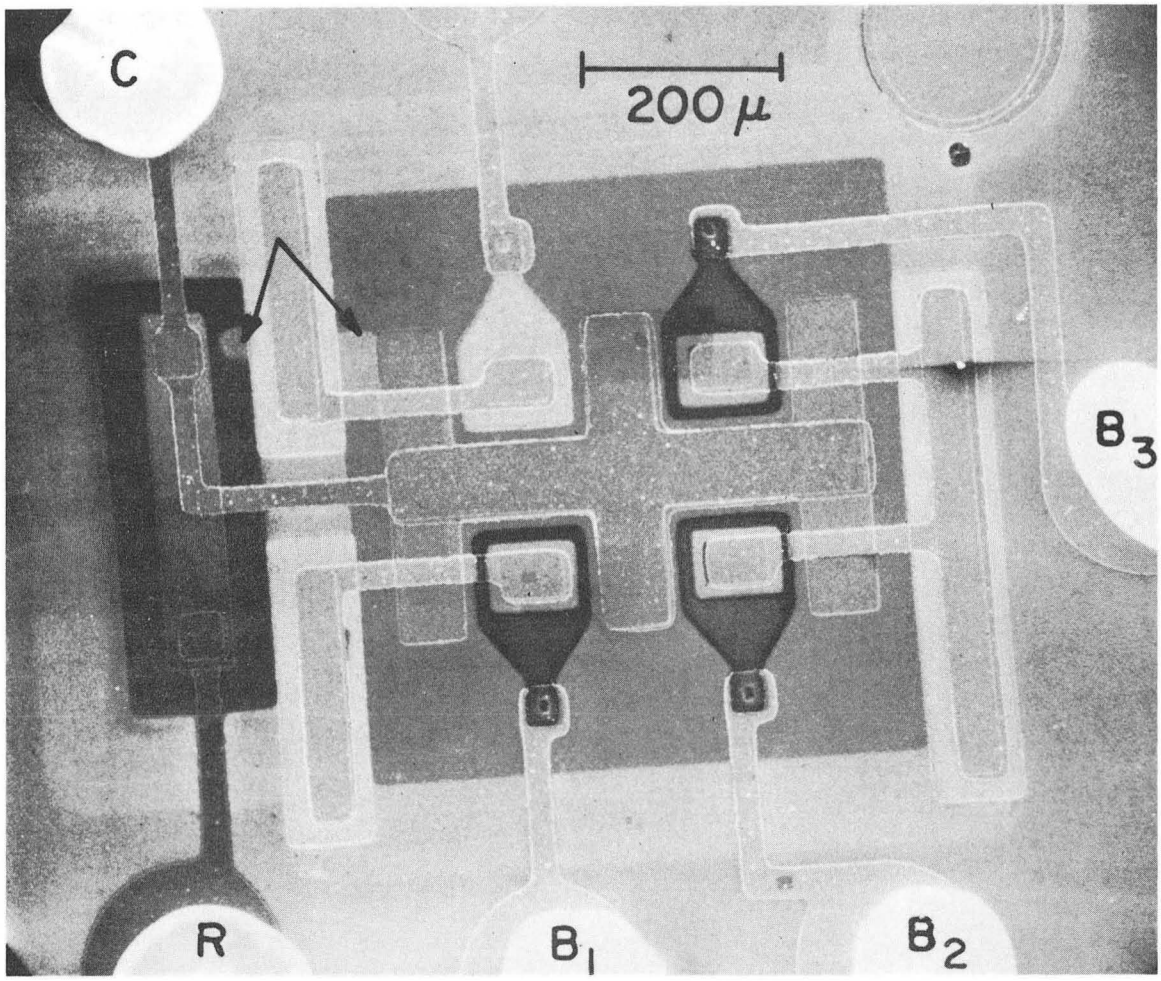

XBB707-3382

Fig. 7.

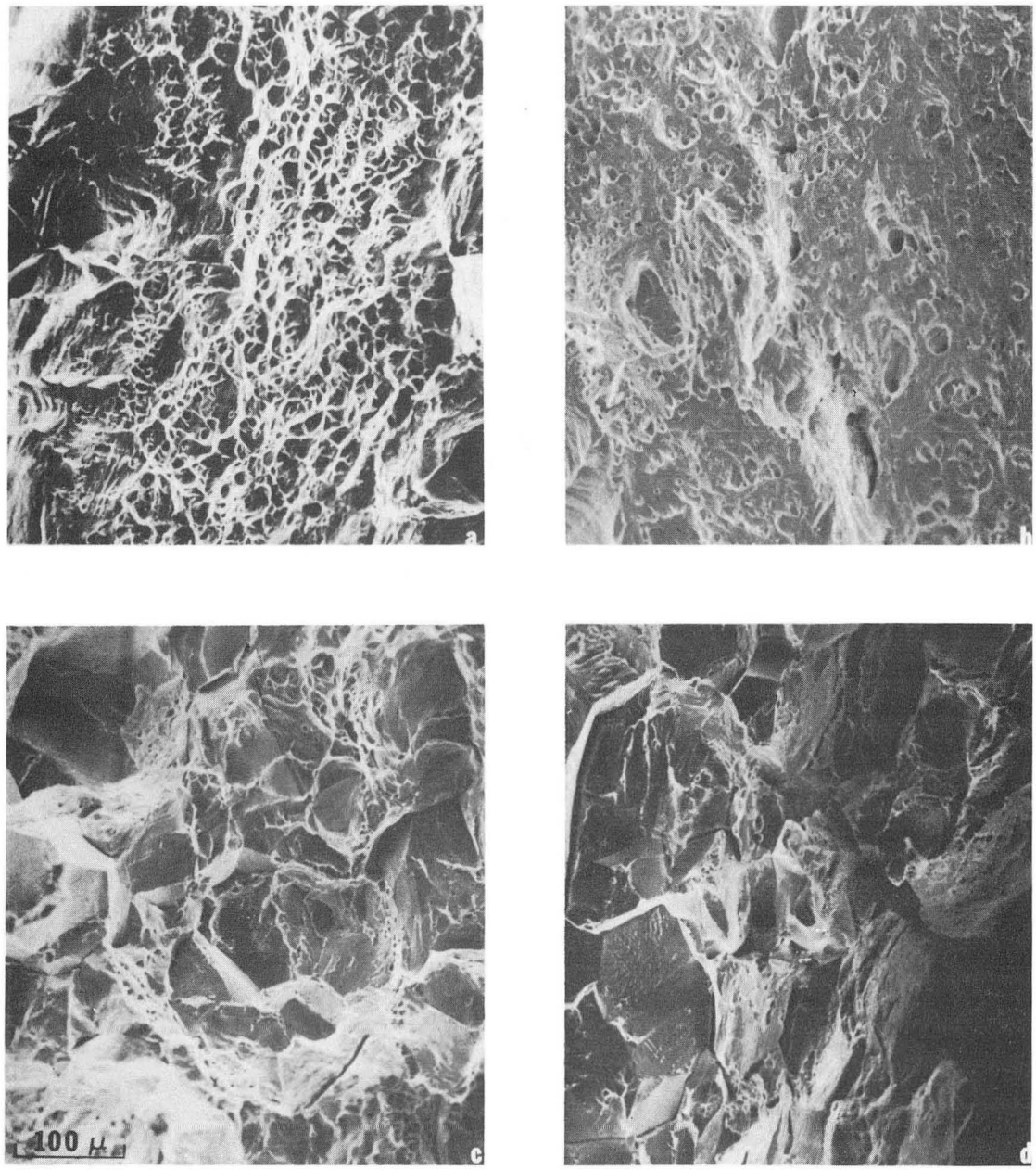

XBB702-1103

Fig.8.

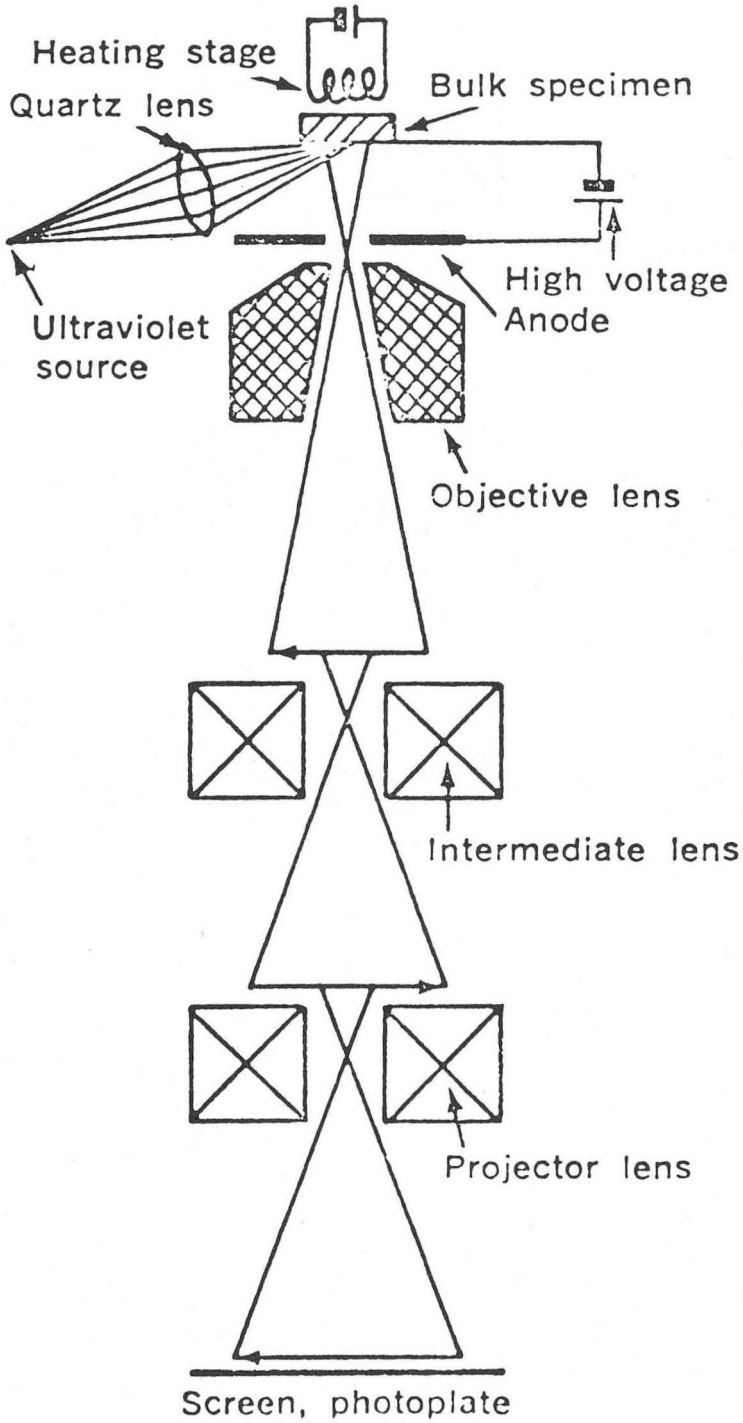

XBL 7011-6933

Fig. 9.

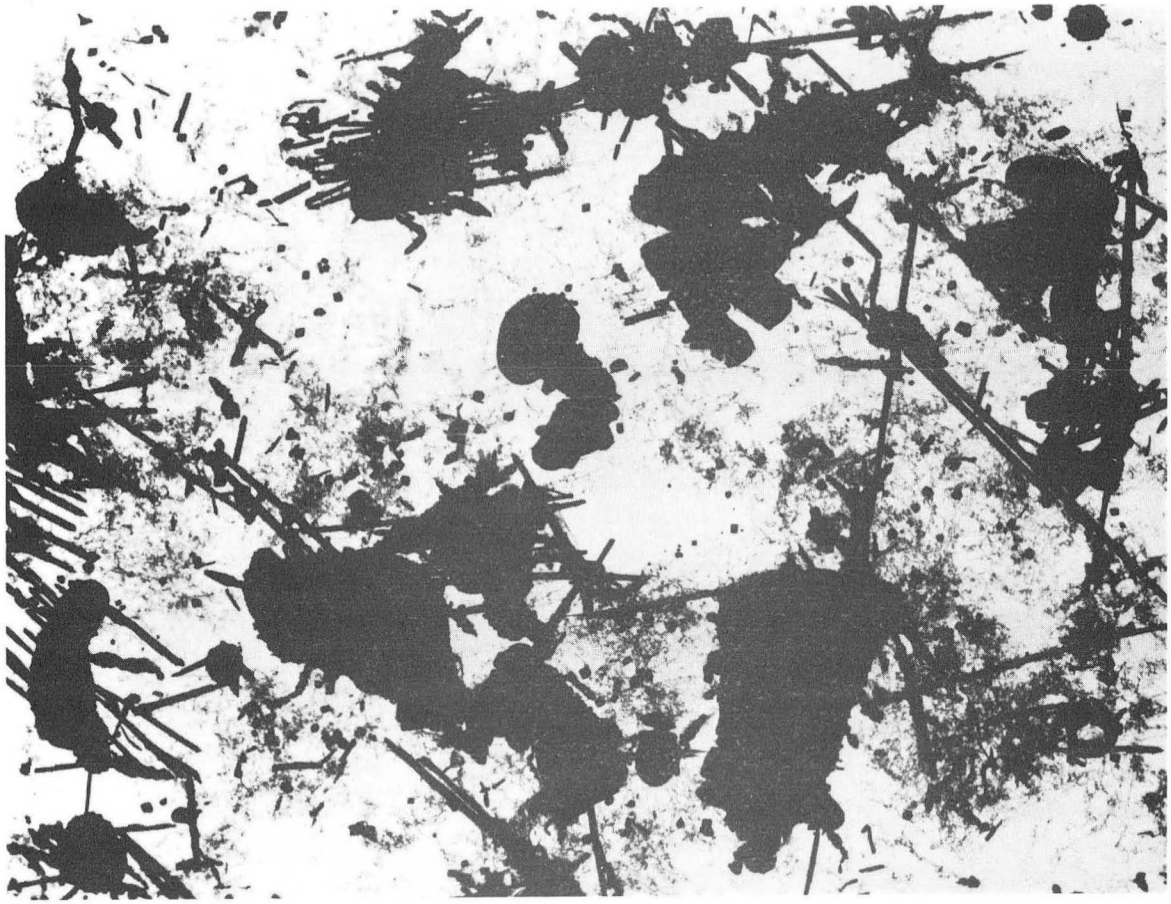

XBB708-3774

Fig. 10.

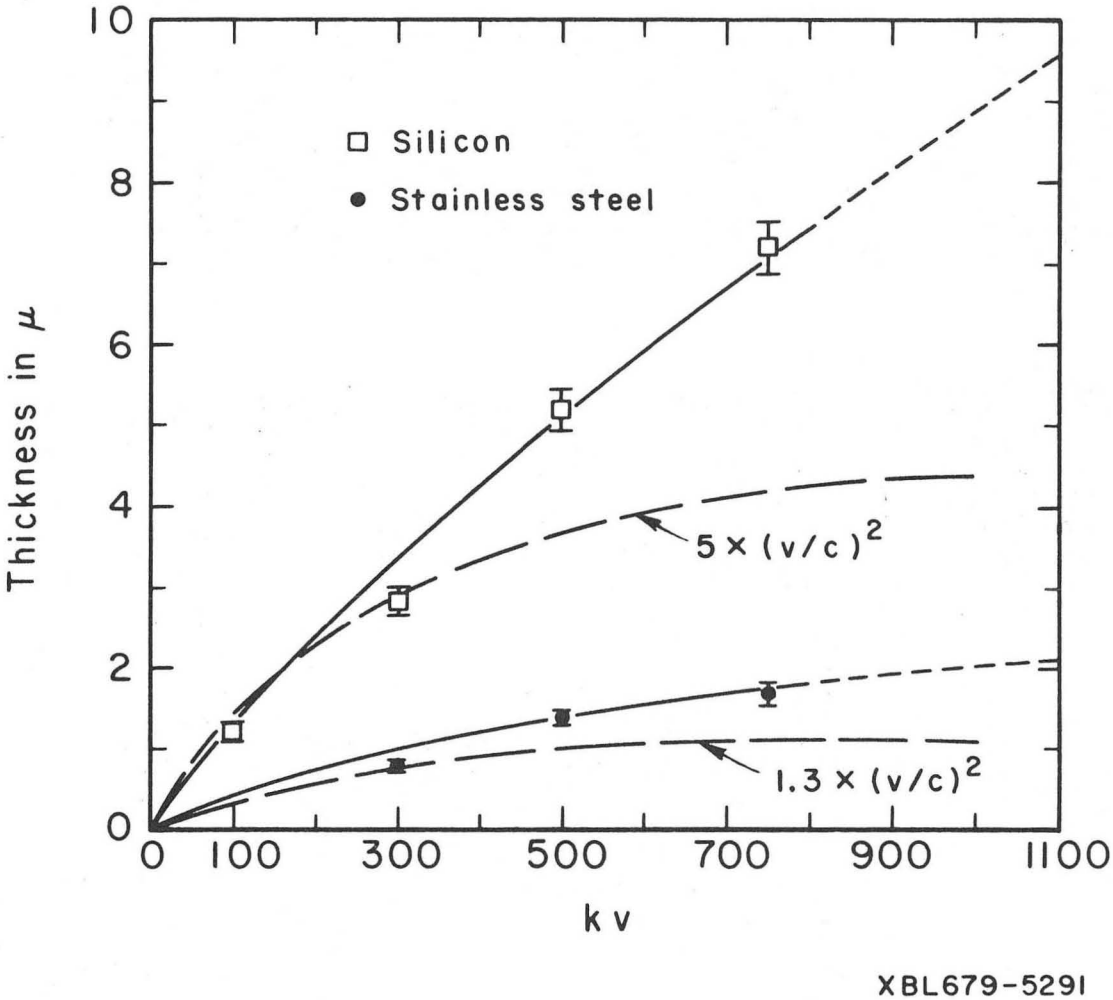
10
8
6
4
2
0
Thickness in μ
□ Silicon
● Stainless steel
5 × (v/c)²
1.3 × (v/c)²
0
100
300
500
700
900
1100
kv
XBL679-5291

Fig. 11a.

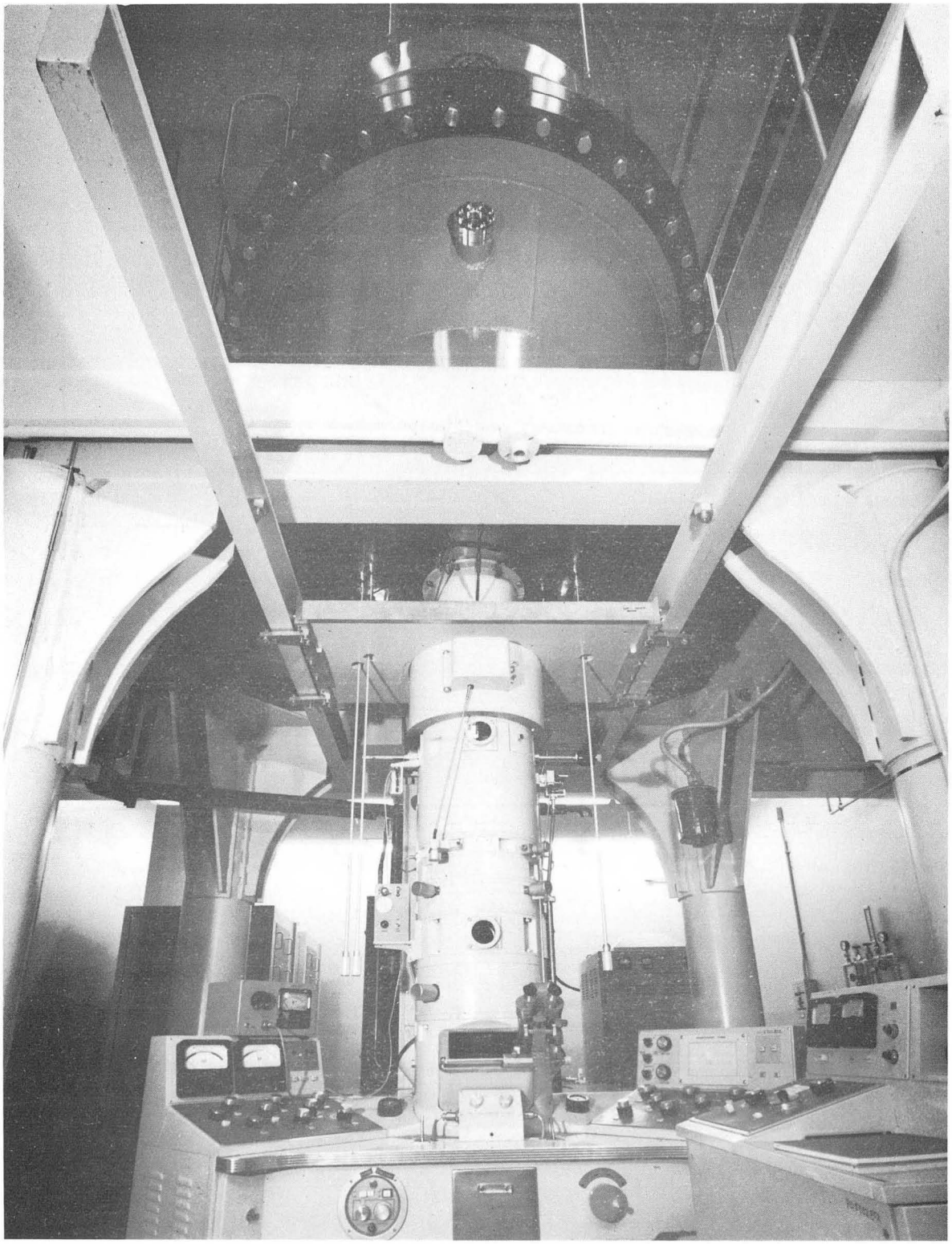

CBB701-360

Fig. 11b.

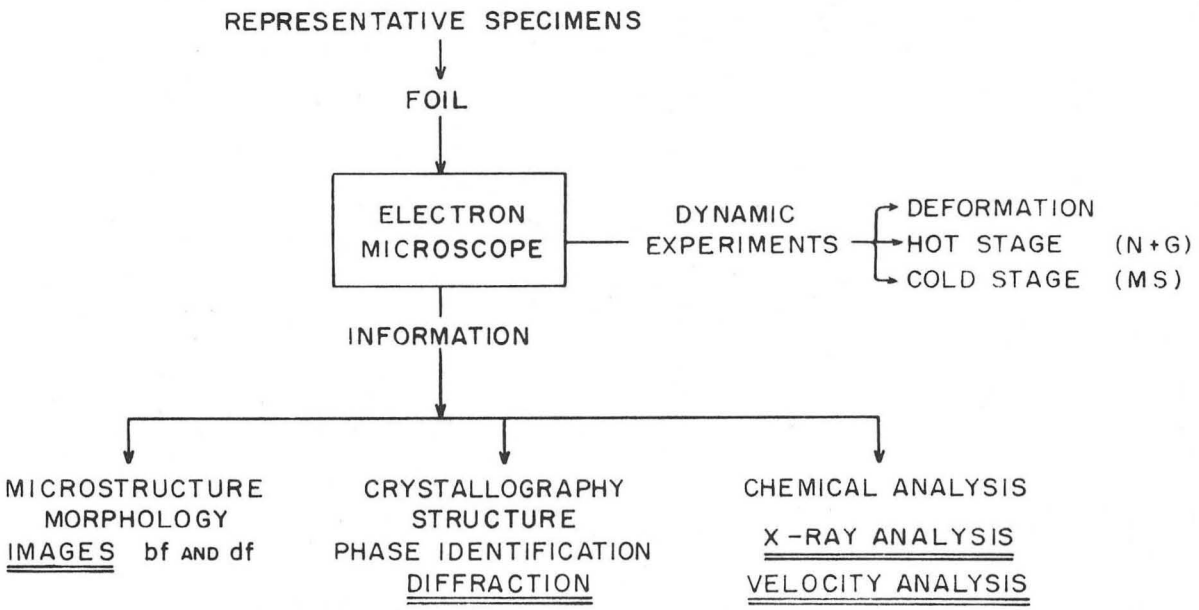

XBL 695-581

Fig. 12.

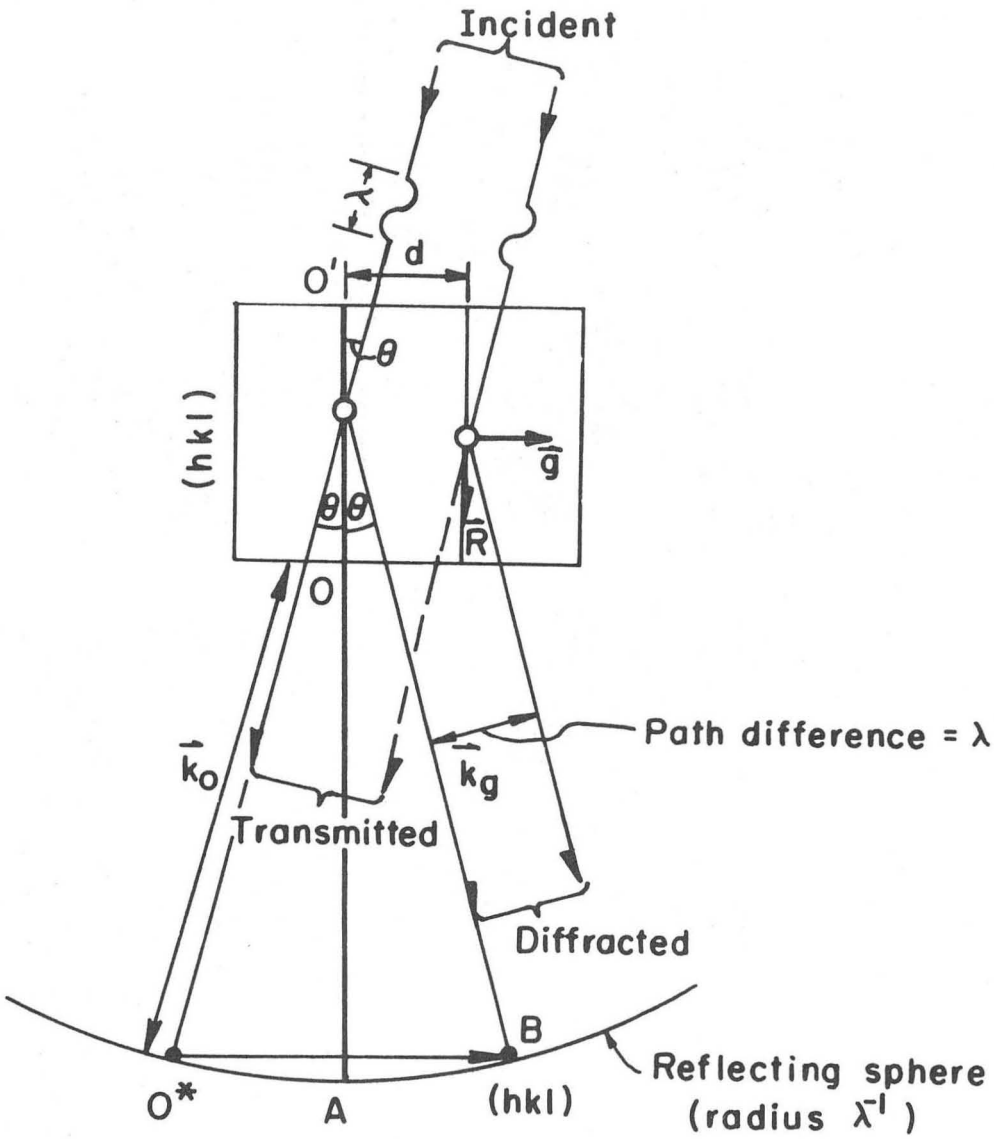
Incident
d
O'
θ
(hkl)
g
θ θ
R
O
Path difference = λ
k_O
k_g
Transmitted
Diffracted
B
Reflecting sphere
(radius λ⁻¹)
O*
A
(hkl)
MU-32006

Fig. 13.

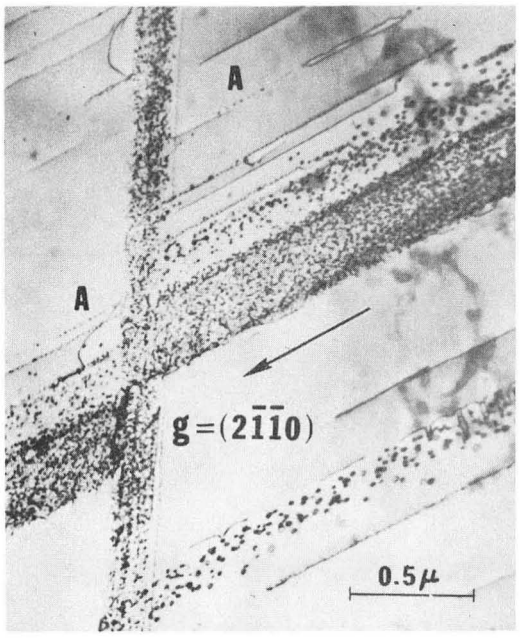

(a)

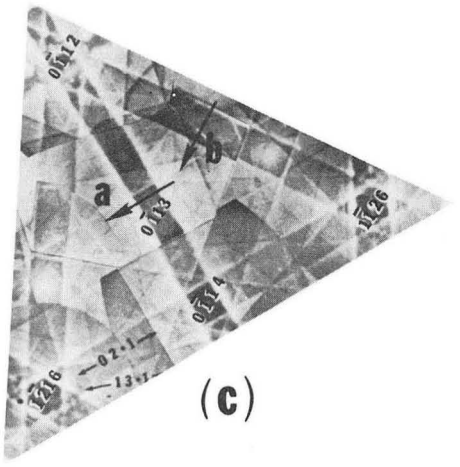

(c)

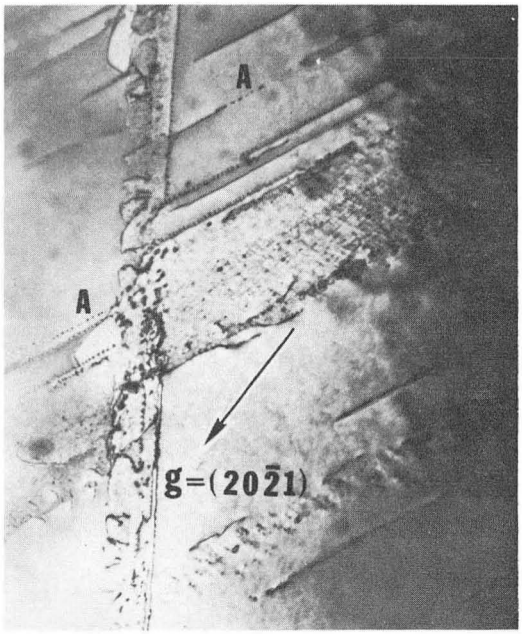

(b)

IM2497

Fig. 14.

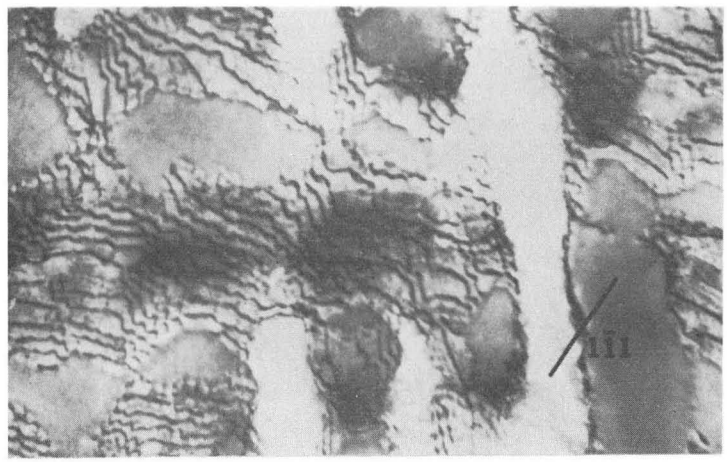

A

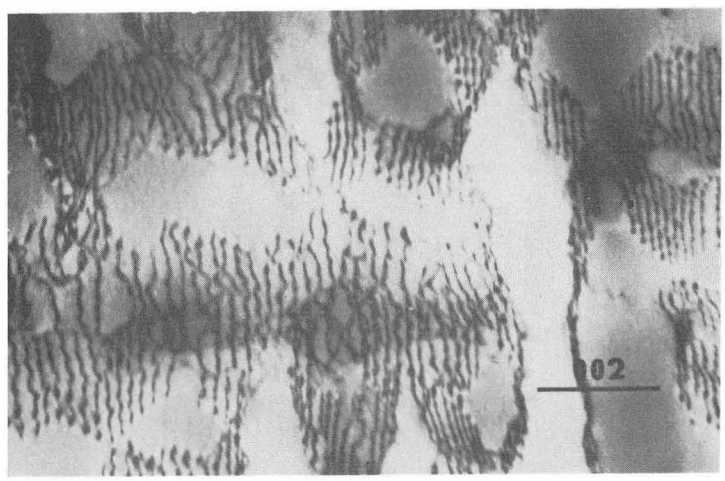

B

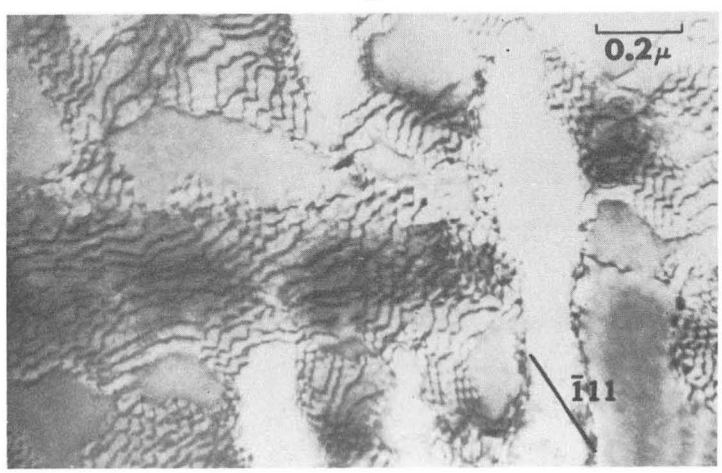

C

XBB 691-244

Fig. 15.

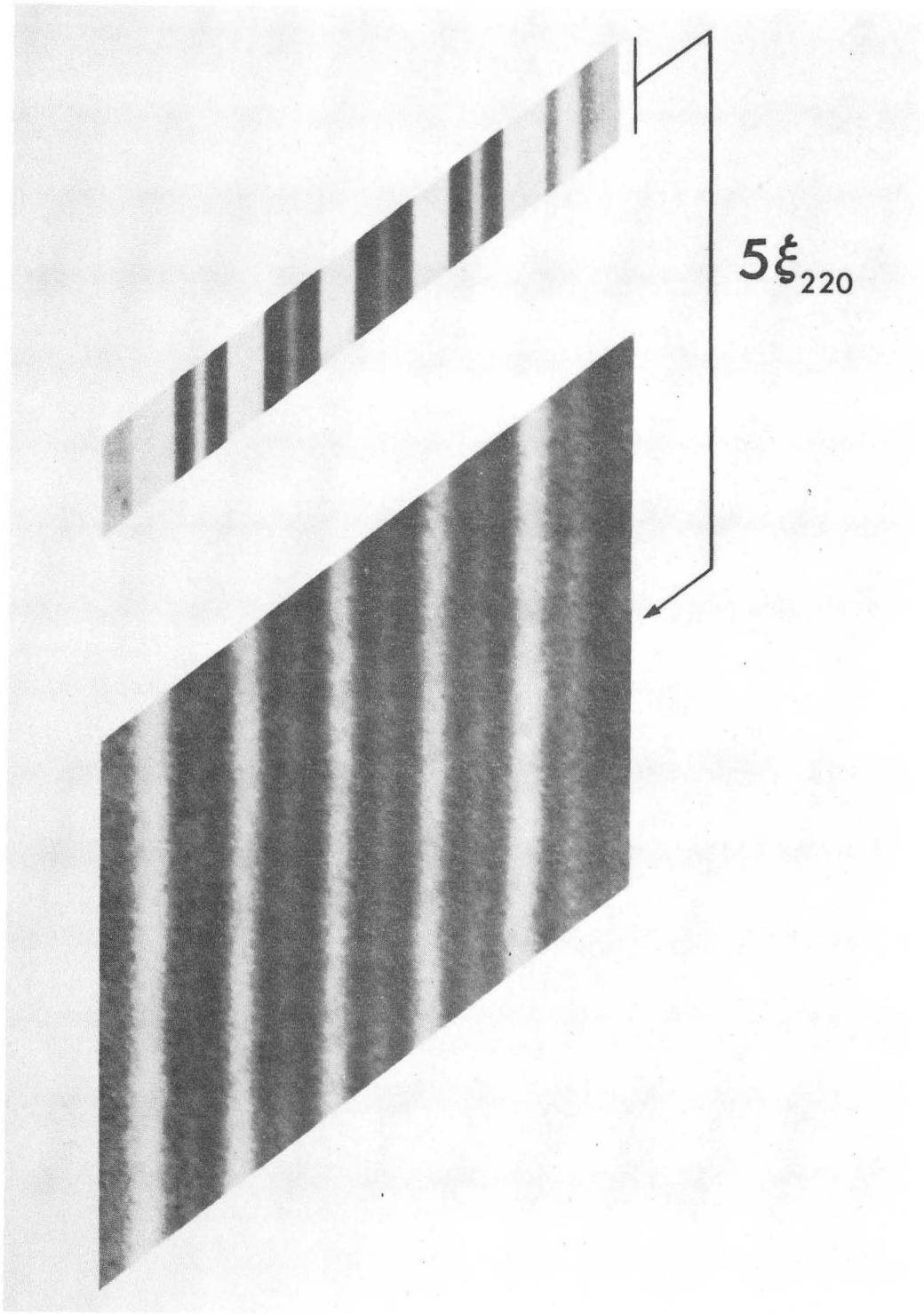

XBB708-3775

Fig. 16.

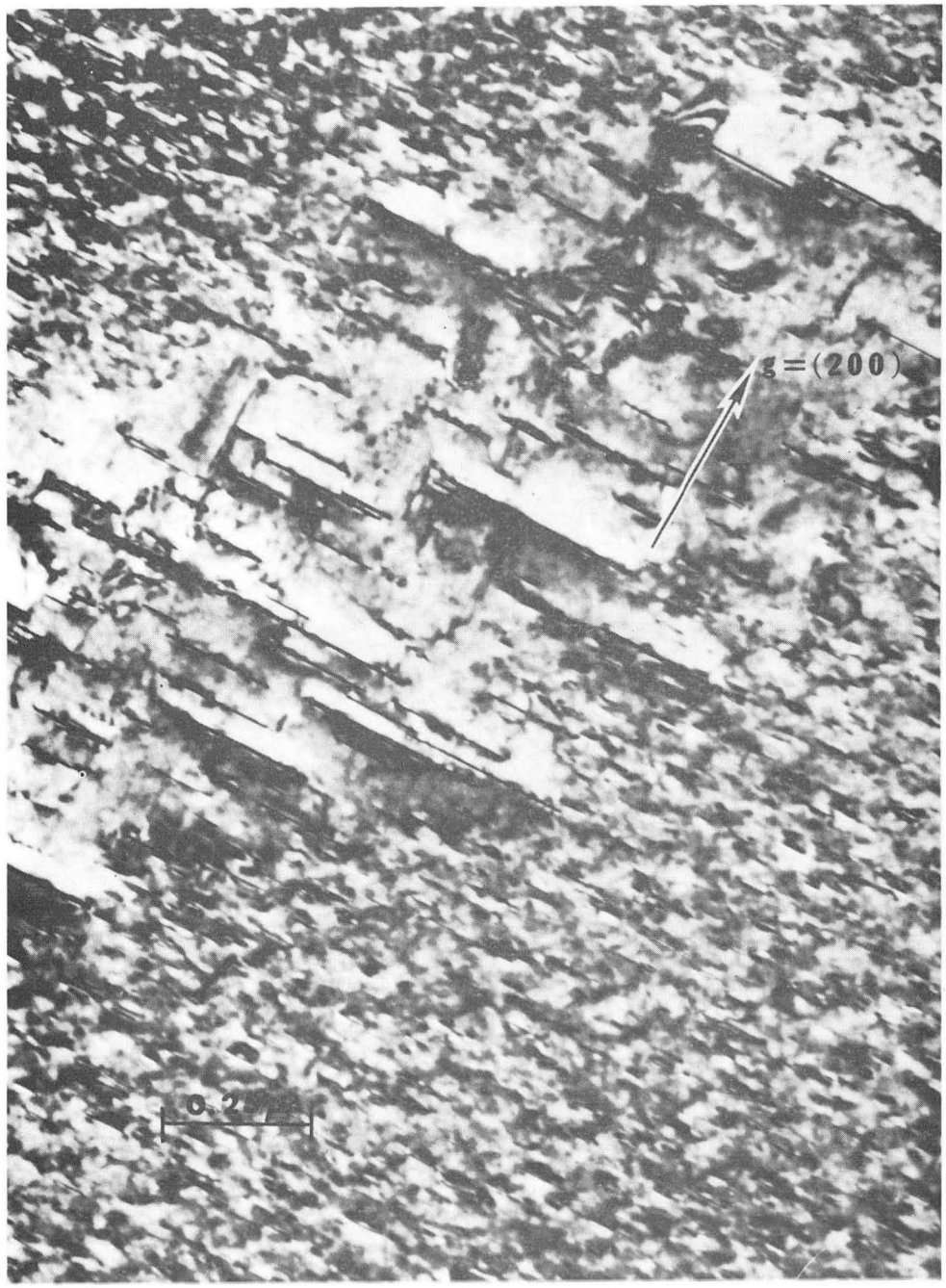

IM2128

Fig. 17.

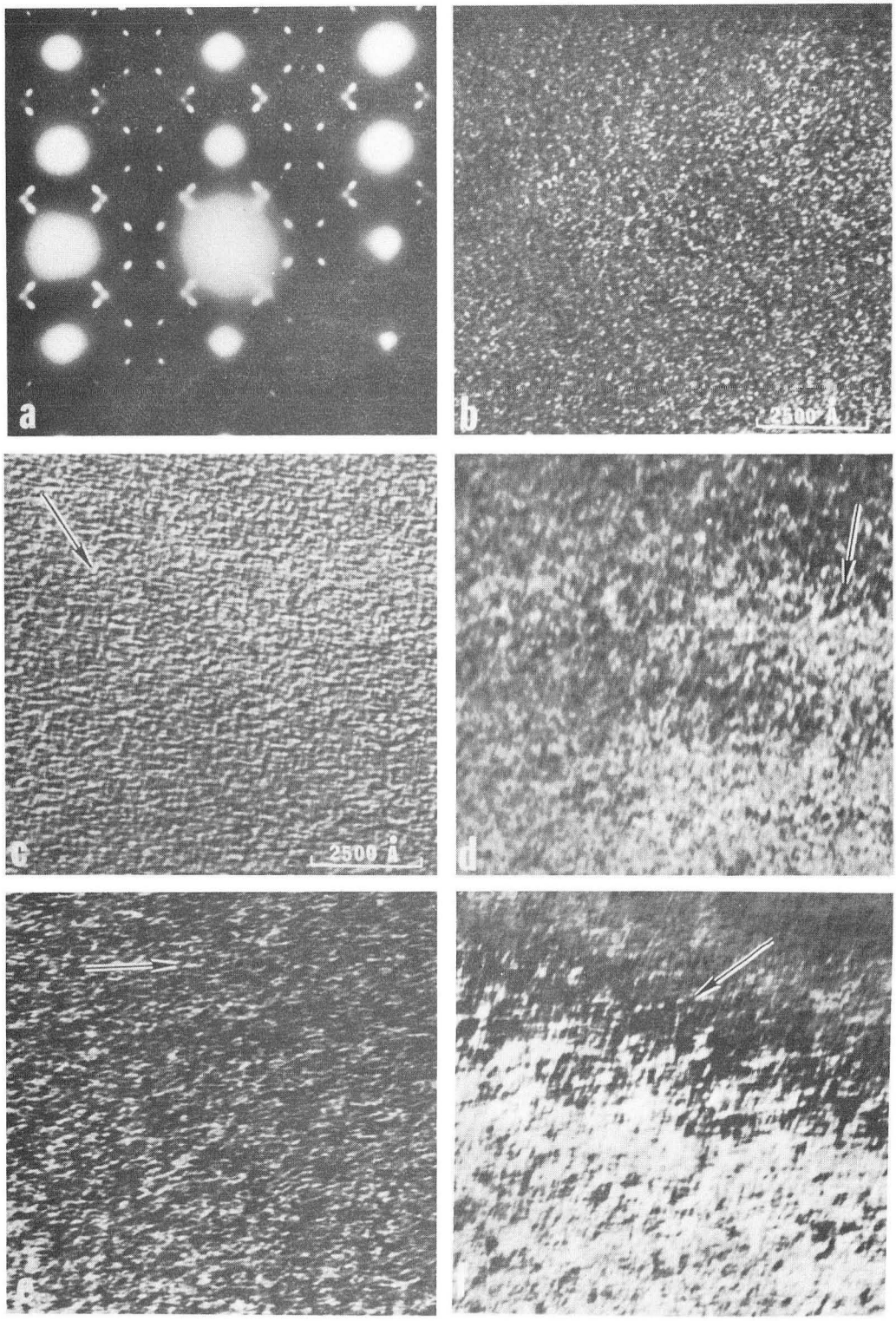

XBB6911-7496

Fig. 18.

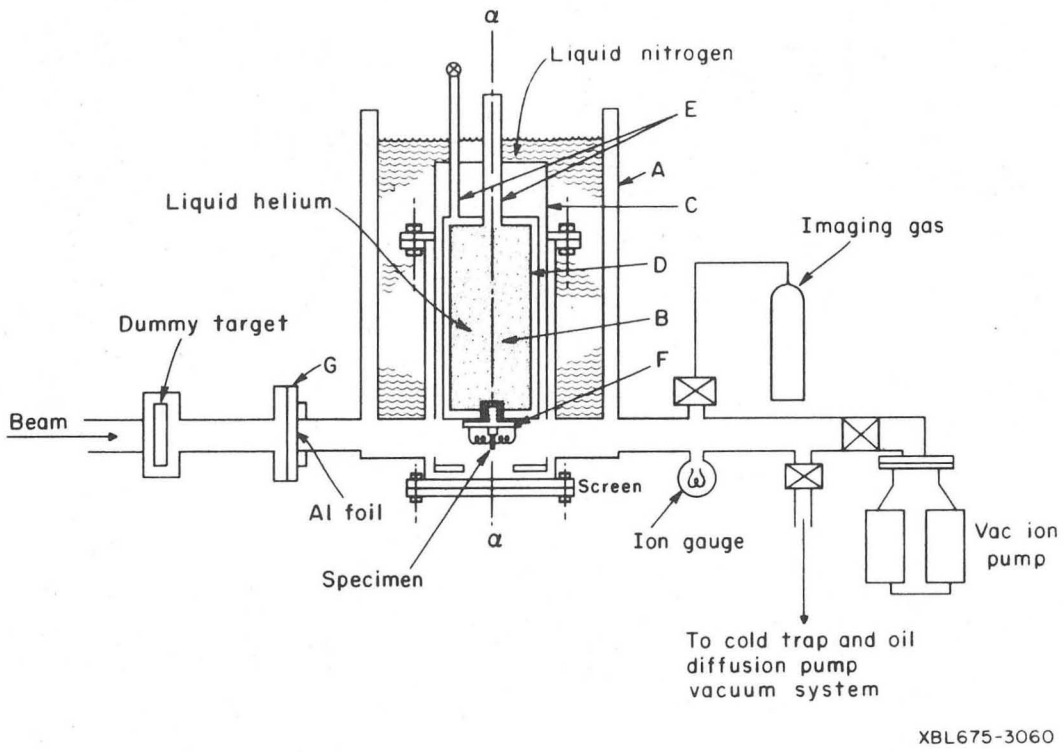
α
Liquid nitrogen
E
A
C
Liquid helium
Imaging gas
D
B
Dummy target
F
G
Beam
Screen
Al foil
α
Ion gauge
Vac ion
pump
Specimen
To cold trap and oil
diffusion pump
vacuum system
XBL675-3060

Fig. 19.

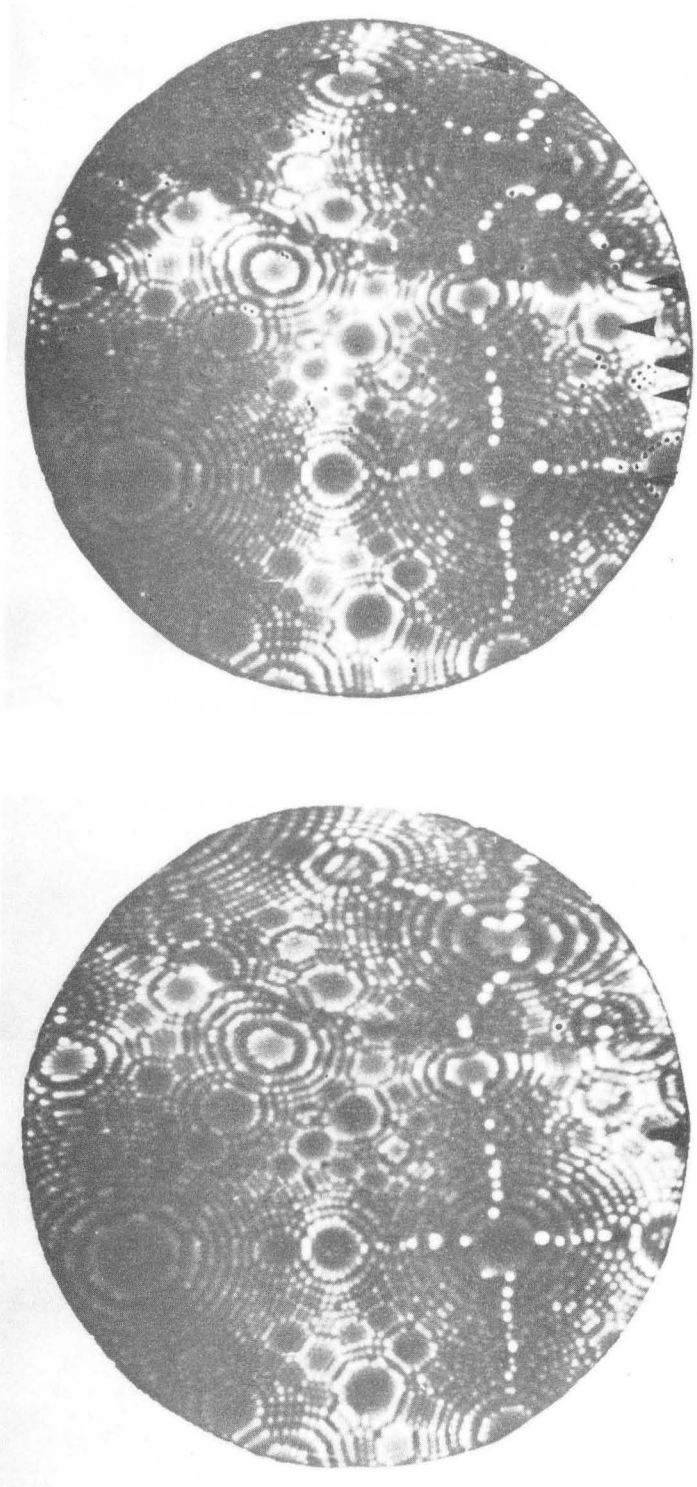

XBB674-2081

Fig. 20.

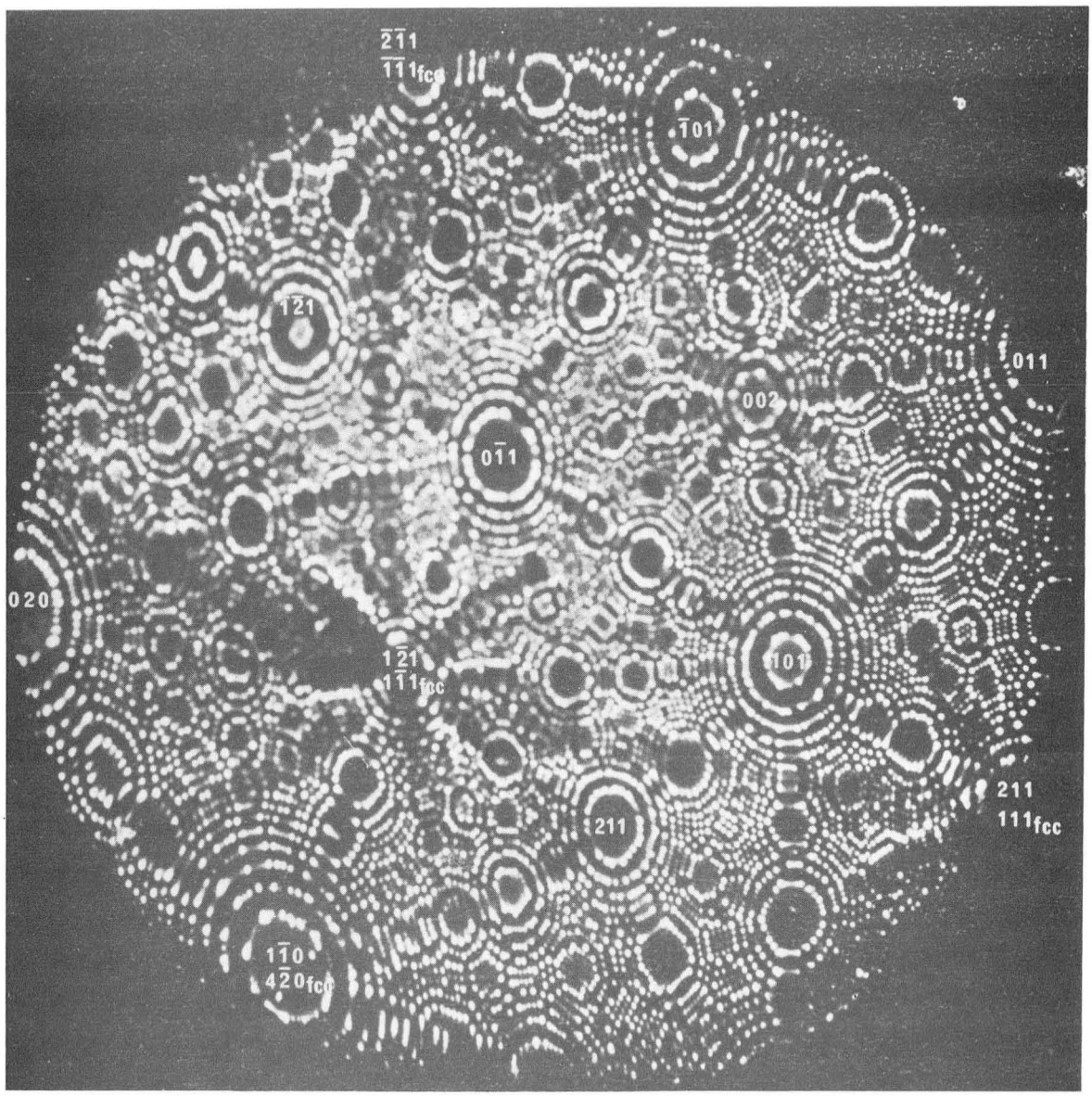

XBB6911-7498

Fig. 2la.

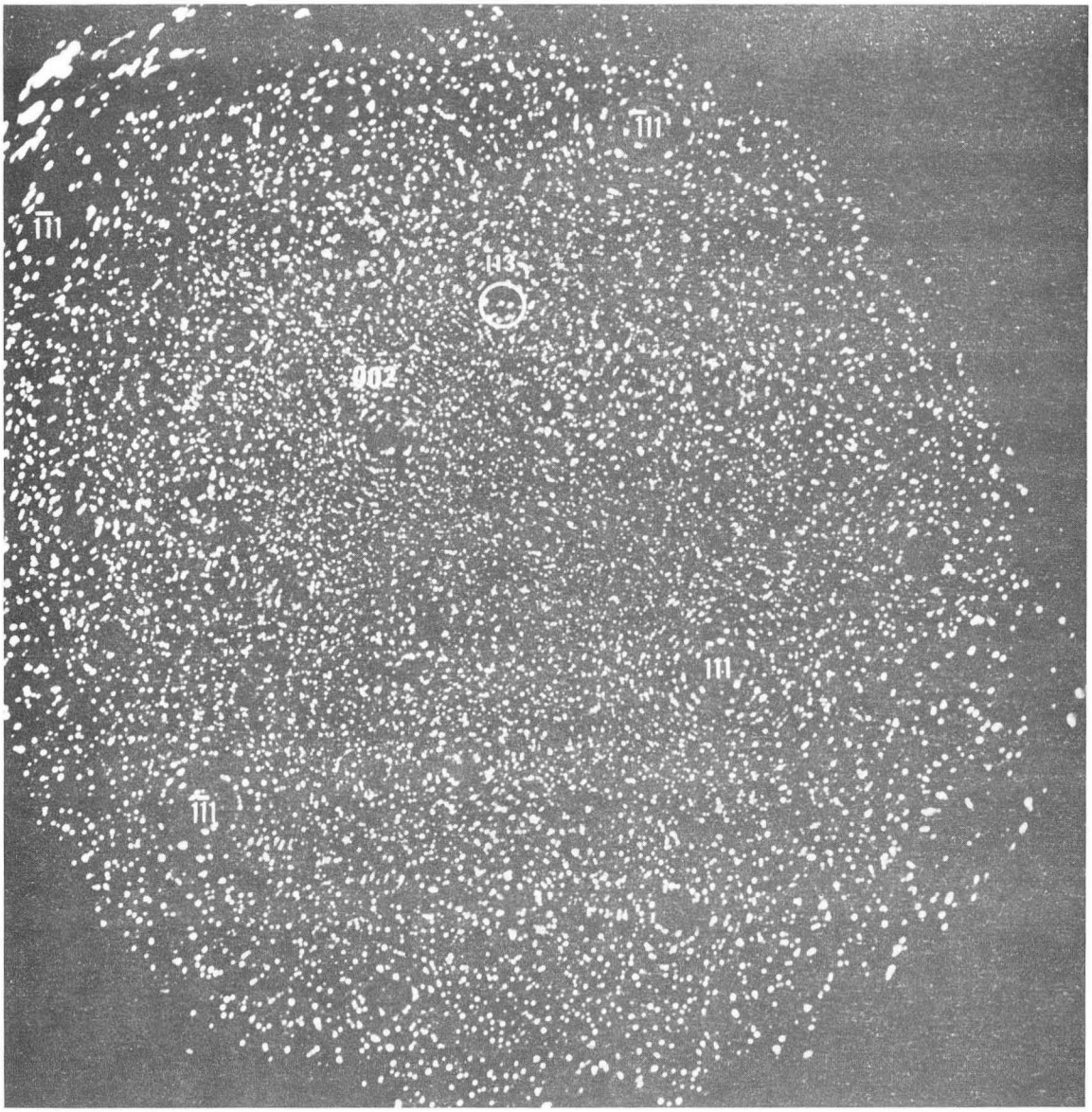

XBB6911-7501

Fig. 21b.

MICROPROBE ANALYSIS OF 64 CU - 27 NI - 9 FE ALLOY

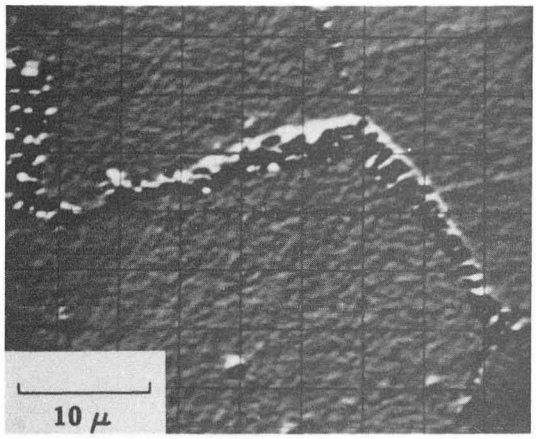

BACK SCATTERED ELECTRON IMAGE

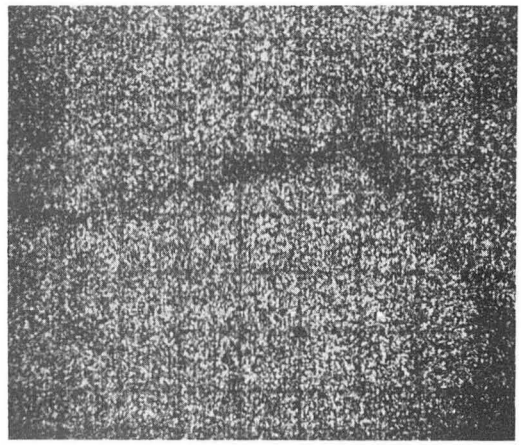

CU K_a RADIATION

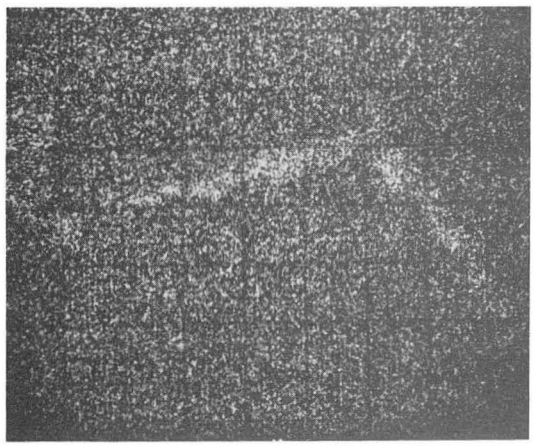

NI K_a RADIATION

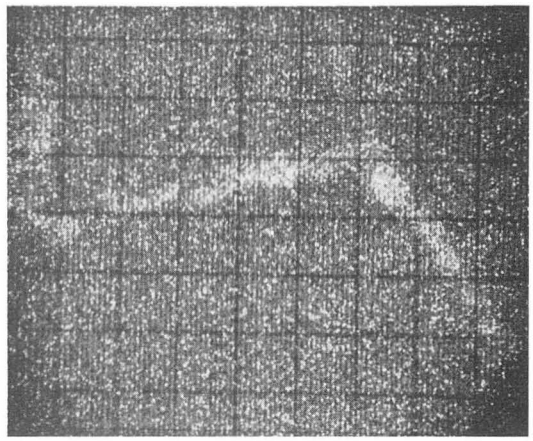

FE K_a RADIATION

XBB707-3327

Fig. 22.

TECHNICAL INFORMATION DIVISION
LAWRENCE RADIATION LABORATORY
UNIVERSITY OF CALIFORNIA
BERKELEY, CALIFORNIA 94720